UNIVERSIDAD DE CHILE
FACULTAD DE CIENCIAS FÍSICAS Y MATEMÁTICAS
DEPARTAMENTO DE INGENIERÍA ELÉCTRICA

ON THE INFLUENCE OF THE NON-WSSUS CONDITION IN THE PERFORMANCE OF IEEE 802.11-BASED CHANNEL ESTIMATORS FOR VEHICULAR COMMUNICATIONS

TESIS PARA OPTAR AL GRADO DE MAGISTER EN CIENCIAS DE LA INGENIERÍA, MENCIÓN ELÉCTRICA

NICOLÁS MATÍAS ORTEGA SILVA

PROFESOR GUÍA:
CESAR AZURDIA MEZA

PROFESOR CO-GUÍA:
CARLOS GUTIERREZ DIAZ DE LEÓN

MIEMBROS DE LA COMISIÓN:
MICHAEL RICE
JORGE SILVA SÁNCHEZ

Este trabajo ha sido parcialmente financiado por Proyecto FONDECYT Iniciacion Grant No. 11160517 y ERANet-LAC Grant No. ELAC2015/T10-0761

SANTIAGO DE CHILE
2020

RESUMEN DE LA TESIS PARA OPTAR
AL GRADO DE MAGISTER EN CIENCIAS
DE LA INGENIERÍA, MENCIÓN ELÉCTRICA
POR: NICOLÁS MATÍAS ORTEGA SILVA
FECHA: 2020
PROF. GUÍA: CESAR AZURDIA MEZA
PROF. CO-GUÍA: CARLOS GUTIERREZ DIAZ DE LEÓN

ON THE INFLUENCE OF THE NON-WSSUS CONDITION IN THE PERFORMANCE OF IEEE 802.11-BASED CHANNEL ESTIMATORS FOR VEHICULAR COMMUNICATIONS

Las redes de comunicación vehiculares que potencialmente podrán mejorar la seguridad vial, están generando un gran interés en la comunidad científica. Ya que algunas de estas redes vehiculares utilizan el medio radio eléctrico para la propagación, la estimación de canal es fundamental. La mayor parte de las técnicas de estimación de canal se diseñan asumiendo que el canal es estacionario en el sentido amplio y que los dispersores están no correlacionados entre si. Estas dos condiciones son llamadas la condición WSSUS para el modelamiento de canal, por sus siglas en inglés. Sin embargo, una serie de campañas de medición llevadas a cabo a través de todo el mundo, sugieren que la condición WSSUS podría no cumplirse en un entorno vehicular.

En este trabajo estudiamos un model de canal de móvil a móvil que es no-WSSUS, como resultado de su lógica de modelamiento. Este modelo de canal permite la incorporación de cambios de velocidad en los móviles. Esta característica particular del modelo de canal seleccionado, lo convierte en un modelo que puede ser apropiadamente usado para simular entornos de propagación vehicular. Caracterizamos estadísticamente el proceso estocástico inducido por el canal, incluyendo la Función de Correlación, la cual permite estudiar el cumplimiento, o no, de las condición WSSUS. Con la correcta caracterización estadística del canal realizada, se caracteriza el efecto Doppler de canales de Radio de Gran Ancho de Banda, como los que se ocupan en el protocolo IEEE 802.11p.

Habiendo estudiado las características estadísticas del modelo de canal seleccionado, se utilizan simulaciones para comparar el rendimiento de tres técnicas de estimación de canal, basadas en el estándar IEEE 802.11p, en términos de su tasa de error de bit (BER). Comparamos los resultados de BER de las diferenres técnicas variando el valor de parámetros relacionados con el efecto Doppler, dígase, la aceleración de los móviles y la distancia entre ellos. Nuestros resultados muestran que las no estacionaridades causadas por el efecto Doppler, son la razón principal de la degradación del rendimiento del sistema. Utilizamos la función de correlación para tener un conocimiento previo de como se comportará el BER en los distintos escenarios. También mostramos que el rendimiento de BER de los esquemas de estimación tiempo-frequencia, son áltamente afectados por la distancia entre los móviles. Sin embargo, éstos esquemas de estimación no son afectados por la aceleración de los móviles. Por otra parte, mostramos que el rendimiento de BER de los esquemas de estimación de dominio del tiempo, no son afectados ni por la distancia entre los móviles, ni por las aceleraciones de estos.

SUMMARY OF THE THESIS TO OBTAIN
THE MASTER'S DEGREE IN ENGINEERING SCIENCE,
MENTION IN ELECTRICAL ENGINEERING
BY: NICOLÁS MATÍAS ORTEGA SILVA
DATE: 2020
ADVISOR: CESAR AZURDIA MEZA
CO-ADVISOR: CARLOS GUTIERREZ DIAZ DE LEÓN

ON THE INFLUENCE OF THE NON-WSSUS CONDITION IN THE PERFORMANCE OF IEEE 802.11-BASED CHANNEL ESTIMATORS FOR VEHICULAR COMMUNICATIONS

Vehicular communication networks that may improve road safety are generating wide interest. As most vehicular networks use the radio frequency medium, channel estimation is crucial. Most channel estimation techniques are designed assuming the wide sense stationary uncorrelated scattering (WSSUS) condition for the channel model. However, several measurement campaigns carried out around the world suggest that the WSSUS assumption might not hold in a vehicular environment.

In this work, we study a mobile to mobile channel model that is non-WSSUS as a result of its modeling approach. This channel model allows incorporating velocity variations on the mobiles. This particular characteristic of the selected channel model turns it into a reference channel model that can be properly used to simulate a vehicular propagation environment. We statistically characterize the stochastic process induced by the channel, including the correlation function, in order to study the fulfilment or not, of the stationary conditions. With the proper statistical characterization of the channel model, we characterize the Doppler Shift of wideband mobile radio channels.

Having studied the statistical characteristics of the reference channel model, we conduct a series of simulations to compare the performance of three IEEE 802.11p-based channel estimation techniques in terms of bit error rate (BER). We compare the BER results of the estimation schemes varying the value of parameters related to the Doppler effect, namely, acceleration of the mobiles and the distance between them. Our results show that the non-stationarities caused by the Doppler effect are the principal reason of the degradation of the system performance. We analyze the four-dimensional time-frequency correlation function to obtain insights on which factors affects the BER performance of a vehicular communication system. Furthermore, we show that the BER performance of time-frequency estimation schemes, such as that of the Spectral Time Averaging technique, is strongly affected by the distance between the mobiles, but not by the accelerations of or the trajectory of these. On the other hand, we show that the BER performance of time interpolation only schemes, such as the Least Square technique, is not affected by the distance between the mobiles or the accelerations of them.

'El mundo es unas cuantas tiernas imprecisiones'
Jorge Luis Borges

Agradecimientos

Más lo único que tengo claro es que, hacía el final de mi vida, solo me quedará una interminable lista de proyectos que no finalicé, un inconmensurable numeramiento de pasiones que no me llegaron a apasionar, y una muy, muy reducida (en comparativa) lista de satisfacciones y bellezas relativas que pude dar por concluidas.

A los y las profesoras de mi etapa como estudiante, a mi familia, amigos y amigas, por engrosar todas estas listas.

Muchisimas gracias.

Table of Contents

Tables Index

Figures Index

Acronyms

4D TF-CF Four Dimensional Time Frequency Correlation Function

AOA Angle of Arrival

AOD Angle of Departure

AWGN Additive White Gaussian Noise

BER Bit Error Rate

CDP Constructed Data Pilots

CP Cyclic Prefix

CSI Channel State Information

CTF Channel Transfer Function

DFT Discrete Fourier Transform

DS Doppler Shift

GI Guard Interval

ICT Information and Communication Technologies

IDFT Inverse Discrete Fourier Transform

IF Instantaneous Frequency

IO Interfering Object

ISI Inter-symbol Interference

ITS Intelligent Transportation Systems

LS Least Square

LTV Linear Time-Varying

MAC Medium Access Control

OBU On-Board Units

OFDM Orthogonal Frequency Division Multiplexing

PHY Physical

PWP Planar Wave Propagation

STA Spectral Temporal Avergaging

SWP Spherical Wave Propagation

V2I Vehicle-to-Infraestructure

V2V Vehicle-to-Vehicle

V2X Vehicle-to-Anything

VCS Vehicular Comunication Systems

WAVE Wireless Access in Vehicular Environments

WLAN Wireless Local Area Network

WSSUS Wide Sense Stationary Uncorrelated Scattering

Chapter 1

Introduction

1.1. Motivation

The use of vehicular communication systems (VCSs) for road safety, traffic control, navigation, and automation applications has gained growing attention from both the industry and the scientific community [1, 2]. The VCS comprise information and communication technologies (ICT) that enable the transmission of information over wireless vehicle-to-vehicle (V2V) and vehicle-to-infrastructure (V2I) radio links. The term V2X is the general label for wireless communication systems that connect vehicles among themselves and the road infrastructure [3]. V2X communications employ any form of V2V and V2I transmission links. In 2010, IEEE defined the 802.11p standard for short-range V2X communications.

The IEEE 802.11p amendment was incorporated in 2012 into the IEEE 802.11 standard for wireless local area networks (WLANs). The 'p' amendment specifies the use of orthogonal frequency division multiplexing (OFDM) for the physical (PHY) layer of V2X communication systems. This PHY-mode is an adaption of other modes of the 802.11 standard (introduced as amendments 'a' and 'g'). Because of the necessities that those modes were fulfilling, they were developed to operate on fixed quasi-static (time-invariant) indoor radio channels (WLANs), where users' mobility is a minor concern. These fixed/static scenarios differ significantly from the ones in a vehicular environment, where users move very fast.

To deal with the high mobility of the vehicles, the design of channel estimation techniques, specifically adapted for the characteristics of V2X radio links, is a priority [4]. An obvious requirement for such estimation techniques is the ability to track the rapidly changing channel state information (CSI). A slow tracking rate can result in imprecise CSI snapshots that may compromise the detection process and the overall system's performance [5]. Recent empirical findings have revealed important challenges for the design of proper channel estimators for VCS. One of these challenges is that the vehicular multipath radio channel does not fulfill the wide-sense stationary uncorrelated scattering (WSSUS) condition. For example, empirical data obtained from measurement campaigns carried out independently in [6] and [7] show that the WSSUS condition is valid only over short time intervals and frequency bandwidths.

The empirical evidence of the invalidity of the WSSUS condition has prompted a large number of research activities aimed at the characterization of non-WSSUS V2X multipath radio channels. Several geometry-based statistical models have been proposed in recent years [8, 9, 10, 11, 12], both with spherical wave propagation (SWP) and plane wave propagation (PWP) modeling approaches. In this work we put our focus on the models presented in [8] and [9]. Both of these models are the only works that deal with the statistical characterization of non-WSSUS V2X channels under the PWP approach available in the literature. The PWP modeling approach permits to have expressions for the second order statistics that are easier to work out. In [8], the authors present a non-WSSUS channel model that assumes constant velocities for both the transmitter and receiver mobile stations. Following an approach similar to the one presented in [8], in [9] the authors present a non-WSSUS channel model that incorporates velocity variations of the mobile stations. In spite of the recent advances in the modeling of non-stationary channels for VCS, the impact of these empirical findings on the system performance has not been deeply studied.

1.2. Problem Statement and Hypothesis

1.2.1. Problem Statement

As we have stated, several works, both theoretical and experimental, have made efforts to characterize the multipath channel of a vehicular environment. However, in the literature, we have not found works done on how the non-WSSUS statistical characteristics would affect the BER performance of the system. As the BER is one of the most important figures of merit in a digital communication system, in this work we study the impact of the non-WSSUS statistics on the system performance. As this subject has not been previously studied, our work contributes to expand the knowledge on how the non-stationary characteristics of the V2X channel affect the transmition of data among vehicles on the move. This knowledge can be used to optimize the PHY layer of the current vehicular communication systems, and thereby, make road safety applications more reliable.

To contribute with the safety concerns of the vehicular networks, in this work we perform a series of experiments in different scenarios that can be considered critical, on the context of a road with vehicles on it. We simulate a single user communication link to study the second-order statistics of the channel models proposed in [8] and [9]. On the same scenario, we also obtain the BER performance of different IEEE 802.11p based channel estimation techniques. The selected channel estimation techniques are well known in the literature [13, 14, 4].

1.2.2. Hypothesis

We establish the hypothesis of the work as follows:

- The non-WSSUS condition in a vehicular communication channel impacts the performance of state-of-the art IEEE 802.11p estimators in terms of the BER.

1.3. Objectives

The objectives of the work are summarized as follows:

- **General objective:** To analyze the second order statistics of a vehicular channel model, under different scenarios, and asses the influence of these statistics on the BER performance of IEEE 802.11-based channel estimators.
- **Particular objectives:**
  - Study the WSSUS condition of the second order statistics of the Geometrical Based Channel Model proposed in [9].
  - Characterize the origins of the non-WSSUS condition of the channel model proposed in [9].
  - Extend the statistical analysis performed on [9] to different propagation conditions.
  - Compare and to analyze the BER performance of time domain channel estimators under a WSSUS model, and on the non-WSSUS model proposed on [9].
  - Compare and to analyze the BER performance of time-frequency domain channel estimators under a WSSUS model, and on the non-WSSUS model proposed on [9].
  - Compare and to analyze the BER performance of time domain channel estimators under the non-WSSUS model proposed on [9], by considering different parameters associated to the Doppler effect, namely, the initial distance between the mobiles and their respective velocities and accelerations.
  - Compare and to analyze BER performance of time-frequency domain channel estimators under under the non-WSSUS model proposed on [9], by considering different parameters associated to the Doppler effect, namely, the initial distance between the mobiles and their respective velocities and accelerations.

1.4. Thesis Structure

The rest of this thesis is structured as follows. In Chapter 2 we briefly review some concepts related to Vehicular Communications Networks, mainly regarding the IEEE 802.11p Communication Standard. A review of some channel estimation techniques that follows this communication protocol is also given in this chapter. On subsequent Chapters, we use the IEEE 802.11p standard and the channel estimation techniques reviewed to perform simulations.

In Chapter 3 we systematically analyze a non-WSSUS channel model that allows velocity variations on the mobiles that are involved in the communication. The statistical characteristics associated with the channel are analyzed and explained. Finally, we study the correlation function of the single ring model proposed on [8], for the specific case that we study in this thesis. This study is done by performing and analyzing numerical simulations on the correlation function.

In Chapter 4 we characterize the Doppler shift for wideband mobile radio channels, as the ones that are used in the IEEE 802.11p standard, and we identify the time-frequency dependency of the Doppler Shift as the cause of the non-stationarities in both time and frequency domains. This chapter is based on the work published in [15].

In Chapter 5 we study the impact of the channel's non-stationarities in an IEEE 802.11p communication system, evaluating the system's BER performance and relating these results to the channel's second-order statistics. This chapter is based on the the work published on [16] and [17]. Finally, in Chapter 6 we summarize our main conclusions and the projected future work.

Chapter 2

Overview of Vehicular Networks

In this chapter, we review concepts associated to vehicular communications, including the specifications of the IEEE 802.11p standard for dedicated short-range communication (DSRC) systems as much as is pertain to our work. We define the general structure regarding the signal model, along with the channel estimation techniques that are used in the analysis of the subsequent chapters. We also review key parameters of the PHY layer of the IEEE 802.11p standard.

2.1. Vehicular Communications

Vehicular communications networks are a new kind of wireless networks that have been prompted by recent advances on wireless communications technologies. These advances aim at enabling ultra reliable and fast communications in short distances. Such capabilities are essential for communications among vehicles, specially for safety applications. Vehicular communications technologies can be classified under the conceptual umbrella of the so called Intelligent Transport Systems (ITS), which are based on V2X technologies [18].

Novel, fast, and reliable communications technologies would allow the development of a series of applications that can be implemented in the context of a vehicular environment. In [19], the applications for vehicular networks are divided in two groups: safety and user applications.

- Safety Applications
  - Accidents: These are intented at warning cars of an accident that has occurred further along the road, thus preventing a pile-up from occurring. A safety application could also be used to give drivers early warnings (about weather or any kind of anomaly that could be happening on the road), and prevent accidents from happening in the first place.
  - Intersections: Driving near and through intersections is one of the most complex challenges that drivers face because two or more traffic flows intersect, and the

possibility of collision is high. The use of early warning applications may reduce the number of accidents that occur in the intersections.

  - Road Congestion: Safety applications also could be used to provide drivers with the best and less congested routes to their destinations. As the traffic is lower, the risk of an accident to happen is reduced.

- User Applications
  - Internet Connectivity: Constant Internet access has become a daily requirement for many people and because many user applications also require Internet connectivity, providing this facility to vehicle occupants on to other applications is important.
  - Peer-to-Peer Applications: To alleviate boredom from long distances, peer-to-peer applications are also an interesting idea for Vehicular Networks. Passengers could share music, movies, and may play online games.

For this framework of applications to work out, novel network architectures have been developed. Vehicular communication architecture essentially relies on two devices: On-Board Units (OBUs), which are transceivers installed in a car to provide the function of the communication, and Road-Side Units (RSUs) which are devised to be implemented on the roadside to provide a series of functions, such as providing information that come from other networks (such as the Internet), act as repeater of a signal that comes from far away cars, among others. OBUs and RSUs vehicular networks are mainly ad-hoc networks, allowing the nodes of the network to communicate between them without a prior infrastructure. Figure 2.1 shows an example of the aforementioned kind of network.

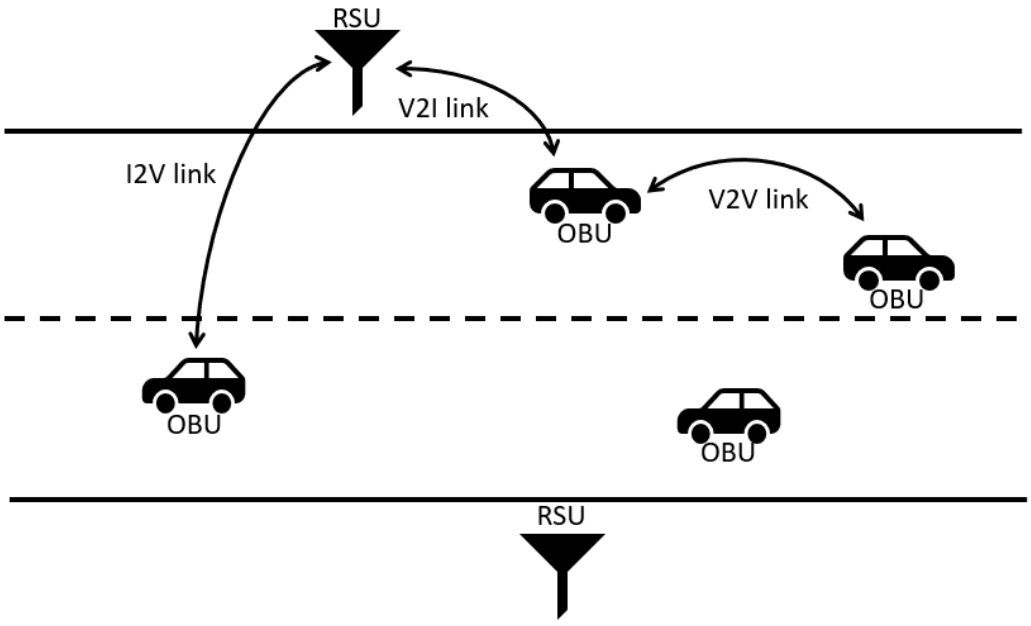

Figure 2.1: Ad-Hoc Vehicle Network Architecture.

As these ideas and concepts for vehicular communications may lead to innovative and important solutions for entertaining and road safety, a framework for the associated vehicular communications systems associated is required. In this thesis, we focus our attention on

the analysis of DSRC technologies, which operate in the 5, 9 GHz frequency band, providing communication support for the road safety and traffic efficiency applications in vehicular networks [18]. DSRC relies on several standards designed for vehicular communications, including the IEEE 802.11p, which defines PHY and Medium Access Control (MAC) layers for Wireless Access in Vehicular Environments (WAVE) [20]. Throughout this work, we focus our attention on the framework provided by the IEEE 802.11p standard for the PHY layer, which is the main subject of the next subsection.

2.2. The IEEE 802.11p Standard

IEEE 802.11 Standard is a set of specifications for the PHY and MAC layers of WLANs [21]. Different amendments of this protocol are used on everyday-use technologies such as Wi-Fi amendments 802.11n and 802.11ac. IEEE 802.11p is the amendment to the IEEE 802.11 standard that establish the specifications for WAVE.

The IEEE 802.11p protocol establishes operation in the 5,9 GHz band with DSRC, which is a technology based on the IEEE 802.11a standard. This 'p' amendment modifies the 'a' one in order to adapt the protocol to the necessities of the vehicular environment. On one side, the bandwidth of the 'a' amendment is halved, resulting in a 10 MHz bandwidth for IEEE 802.11p. Carrier spacing is also reduced by half in comparison to the 802.11a, as IEEE 802.11p has a 0,156 MHz space between carriers. In the time domain, the symbol length is increased to 8 μs. In general, 802.11p doubles all the OFDM time domain parameters of 802.11a, resulting in a transmission rate reduced by half compared to the 'a' amendment [21]. These specifications are summarized in Table 2.1. IEEE 802.11p also specifies its own distribution for the use of the carriers on the OFDM symbol.

Table 2.1: IEEE 802.11p Standard PHY specifications [20].

Parameter	**Value**
Bandwidth	10 MHz
Subcarrier frequency spacing	0,156 MHz
Guard interval duration	1,6 μs
OFDM symbol duration	8 μs
Symbols per OFDM symbol	80
Short training symbols duration	1,6 μs
Total duration of short training symbols	16 μs (10 symbols)
Long training symbols duration	6,4 μs
Total duration of long training symbols	12,8 μs (2 symbols)
Total duration of the preamble	32 μs

The IEEE 802.11p Standard specifies the distribution in the frequency domain of the 64 OFDM subcarriers. According to the standard, 52 subcarriers are used for data and pilot purposes. Figure 2.2 details the arrangement of the 64 carriers of a single OFDM symbol. Data subcarriers are numbered from -26 to -1 and from 1 to 26. IEEE 802.11p also specifies

the use of subcarriers −21, −7, 7 and 21 as pilots subcarriers. These pilot subcarriers are meant to be used for channel estimation, as in IEEE 802.11a. Finally, the IEEE 802.11p protocol reserves twelve null subcarriers as guards bands, to prevent sub- and oversampling effects. The DC subcarrier, numbered with 0, is also a null subcarrier.

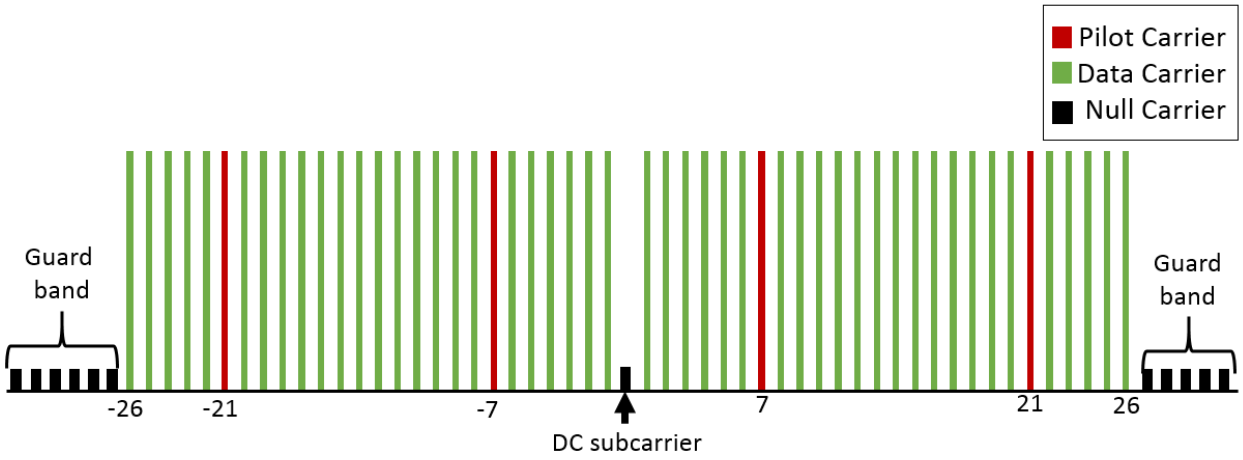

Figure 2.2: OFDM sub-carrier distribution defined in IEEE 802.11p.

Finally, Table 2.2 shows the Modulation Schemes that are considered in the IEEE 802.11p standard. Table 2.2 also shows the coding rates and the corresponding data rates for each modulation.

Table 2.2: IEEE 802.11p Modulation Schemes and Data Rates [20].

Modulation	**BPSK**		**QPSK**		**16-QAM**		**64-QAM**	
Coding Rate	1/2	3/4	1/2	3/4	1/2	3/4	2/3	3/4
Data Rate [Mbps]	3	4,5	6	9	12	18	24	27

2.3. Signal Model of the IEEE 802.11p Data Frame

2.3.1. System Description

For the analysis presented in this thesis, we consider an OFDM signal characterized in the frequency-domain by the baseband-equivalent blockwise input-output relationship

$$Y_{\mathrm{i}}(k) = H_{\mathrm{i}}(k)\, X_{\mathrm{i}}(k) + N_{\mathrm{i}}(k), \tag{2.1}$$

for $\mathrm{i} = 0, 1, \ldots M$, and $k = 0, 1, \ldots, N-1$, where $X_{\mathrm{i}}(k)$ and $Y_{\mathrm{i}}(k)$ are the transmitted and received signals, respectively, for the ith OFDM symbol (signal block) and the kth subcarrier. $H_{\mathrm{i}}(k)$ and $N_{\mathrm{i}}(k)$ stand for the channel frequency response and the additive white Gaussian noise (AWGN) at the kth subcarrier and ith OFDM symbol, respectively.

Figures 2.3 and 2.4 show generalized block diagrams of the OFDM transmitter and receiver, respectively, that will be considered for the analysis presented in this thesis. In these diagrams, uppercase letters stand for signals and systems in the frequency domain, while lowercase letters denote time-domain signals and systems. In Fig. 2.3, data is modulated into some of the constellation defined in Table 2.2. The transmitted symbol block $X_{\mathrm{i}}(k)$ is obtained after the insertion of the pilot subcarriers, and then is fed to an Inverse Discrete Fourier Transform (IDFT) block of $N = 64$ points (subcarriers). With the time domain signal $x_{\mathrm{i}}(n)$ obtained, a Cyclic Prefix (CP) is added to the transmitted signal, following the specifications of the IEEE 802.11p standard, in order to prevent inter-symbol interference (ISI). To this extended version of $x_{\mathrm{i}}(n)$, the IEEE 802.11p preamble is added and then the signal is transmitted to the communication channel $H_{\mathrm{i}}(k)$. The structure of the preamble is the subject of a subsequence section.

Figure 2.4 shows a generalized block diagram of the IEEE 802.11p receiver. The ith OFDM symbol obtained after cyclic prefix removal is denoted by $y_{\mathrm{i}}(n)$. This symbol is fed to a Discrete Fourier Transform (DFT) block of $N = 64$ points. The output of this block is the signal $Y_{\mathrm{i}}(k)$ defined in (2.1). The DFT is followed by the channel estimation and equalization blocks, which are of paramount importance for a robust data detection. The estimate of $H_{\mathrm{i}}(k)$ generated by the channel estimation block is denoted by $\hat{H}_{\mathrm{i}}(k)$. The received signal $Y_{\mathrm{i}}(k)$ and the channel estimate $\hat{H}_{\mathrm{i}}(k)$ serve as input parameters for the equalization block, and the output of this later block, $\hat{S}_{T,\mathrm{i}}(k)$, serves as the input of the demapping block. This block estimates, through a hard-decision process, which symbol of the constellation was transmitted. This decision feds both to the channel estimate block, as some channel estimation techniques use this information, and to the demodulation block in order to obtain the received data.

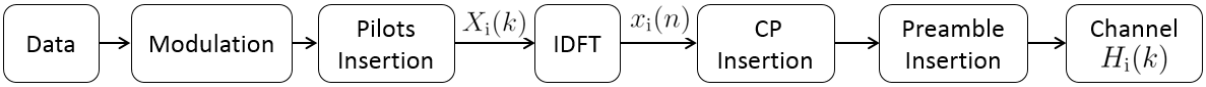

Figure 2.3: Generic vehicular communication transmitter.

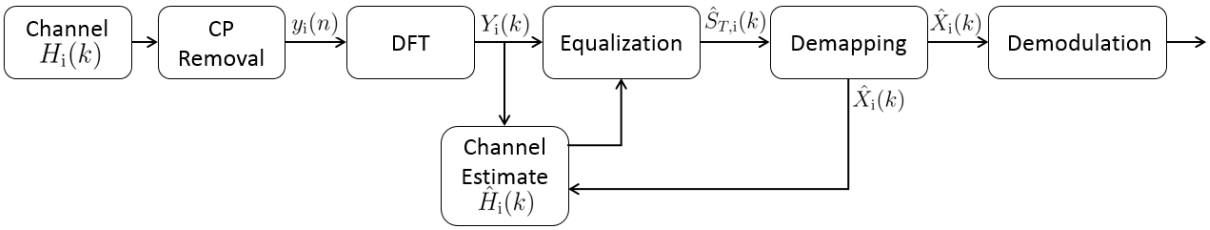

Figure 2.4: Generic vehicular communication receiver.

2.3.2. IEEE 802.11p Preamble Structure

Figure 2.5 shows the structure of the preamble of an IEEE 802.11p packet. The preamble includes short and long training symbols. Short training symbols (t_1 to t_{10}) located at the beginning of every packet are used for synchronization. On the other hand, long training

symbols T_1 and T_2 are used for fine synchronization and channel estimation. $GI2$ stands for the combined double duration Guard Interval (GI) that precedes the two long training symbols. Following the signal model in (2.1), we will denote the transmitted (and received) OFDM signal block associated with the two long training symbols by $X_{T_1}(k)$ and $X_{T_2}(k)$ ($Y_{T_1}(k)$ and $Y_{T_2}(k)$).

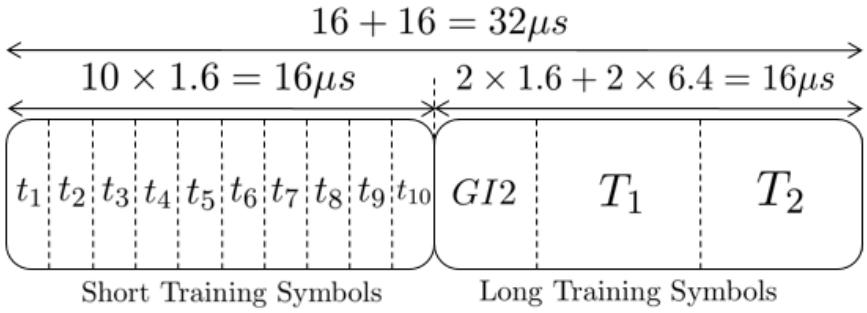

Figure 2.5: IEEE 802.11p packet preamble.

Even though it is included on the standard, the use of the pilot subcarriers shown in Fig. 2.2 for estimation purposes has been discarded by the channel estimation techniques that have been analyzed in this work. This is because the use of only four pilot carriers is not enough to deal with the harsh propagation environment caused by the high mobility of the communication nodes in vehicular communications [4]. Finally, perfect synchronization between the transmitter and receiver is assumed. As a consequence, the use of short training symbols t_1-t_{10} for synchronization purposes is beyond the scope of this work.

2.4. Channel Estimation Techniques

Having clear the structure of the signal model and preamble presented in subsections 2.3.1 and 2.3.2 respectively, in this section, we present the channel estimation techniques that are going to be evaluated with the channel model that is going to be presented in chapter 3, which is a non-stationary one. The studied channel estimation techniques are completely based on the IEEE 802.11p protocol, as they do not change the structure of the package presented in section 2.3.2.

Channel estimation techniques that follow the IEEE 802.11p standard frame structure is a topic that has prompted a lot of research. A good survey and overview of most of the existing works in the field can be found in [4]. In this work, authors present a complete analysis of channel estimation techniques, both that follow the IEEE 802.11p protocol packet structure and the ones who do not, rating their performance and computational complexity. From the techniques given in the survey, in this thesis we study the Least Squares (LS) estimation, the Spectral Temporal Averaging (STA) estimation, and the Constructed Data Pilots (CDP) estimation technique, as these techniques are a common comparison point for other works (see [22], [23], [24], among others).

2.4.1. Least Squares Estimation

The LS estimator uses the long training symbols T_1 and T_2 to formulate a channel estimate, which is then used to equalize all data symbols in the packet [14]. The time-domain channel-corrupted symbols $y_{T_1}(n)$ and $y_{T_2}(n)$ are demodulated with a $N = 64$-point DFT such that,

$$Y_{T_1}(k) = \sum_{n=0}^{N-1} y_{T_1}(n) \mathrm{e}^{-jnk(2\pi/N)}, \quad k = 0, 1, \ldots, N-1, \tag{2.2}$$

$$Y_{T_2}(k) = \sum_{n=0}^{N-1} y_{T_2}(n) \mathrm{e}^{-jnk(2\pi/N)}, \quad k = 0, 1, \ldots, N-1. \tag{2.3}$$

$Y_{T_1}(k)$ and $Y_{T_2}(k)$ denote the received frequency-domain symbols at subcarrier k for training symbols T_1 and T_2, respectively. Because the two training symbols are identical, the LS estimation for the channel frequency response is given by

$$\hat{H}_{LS}(k) = \frac{Y_{T_1}(k) + Y_{T_2}(k)}{X_{T_1}(k) + X_{T_2}(k)}, \tag{2.4}$$

where $X_1(k)$ and $X_2(k)$ denote the frequency-domain training symbols at subcarrier k, respectively. This channel estimate is then applied to the incoming data symbols. The ith received data symbol $y_{R,\mathrm{i}}(n)$, after CP removal, is demodulated and the frequency-domain symbol is given as

$$Y_{R,\mathrm{i}}(k) = \sum_{n=0}^{N-1} y_{R,\mathrm{i}}(n) \mathrm{e}^{-jnk(2\pi/N)}, \quad k = 0, 1, \ldots, N-1. \tag{2.5}$$

A zero-forcing equalization process is employed, using the estimation obtained on (2.4), in order to obtain an estimate version of the ith transmitted signal,

$$\hat{S}_{T,\mathrm{i}}(k) = \frac{Y_{R,\mathrm{i}}(k)}{\hat{H}_{LS}(k)}. \tag{2.6}$$

$\hat{S}_{T,\mathrm{i}}(k)$ is then used to decide which symbol of the constellation was transmitted, and then demodulate the data. The above described process is repeated for every data symbol in the package. It is clear that for a sufficiently large number of OFDM data symbols after the preamble, LS estimation is quickly outdated. Moreover, as we have discussed, V2X communications are characterized by highly dynamic environments, needing a constantly updated CSI.

2.4.2. Spectral Temporal Averaging Estimation

The STA estimation was originally presented in [13] as a technique that could fulfill the CSI tracking requirement of V2X communications. It modifies the LS equalization of (2.6) as follows,

$$\hat{S}_{T,\mathrm{i}}(k) = \frac{Y_{R,\mathrm{i}}(k)}{\hat{H}_{STA,\mathrm{i}-1}(k)}, \tag{2.7}$$

where $\hat{H}_{STA,\mathrm{i}-1}(k)$ is the previously estimated channel response. For the first data symbol of the package, $\hat{H}_{STA,\mathrm{i}-1}(k)$ corresponds to the estimation done on (2.4). Equation (2.7) differs from (2.4) because now the channel estimate dynamically changes as a function of the symbol number i. To update the channel estimate, the channel is first estimated at each subcarrier such that

$$\hat{H}'_{STA,\mathrm{i}}(k) = \frac{S_{R,\mathrm{i}}(k)}{\hat{X}_{\mathrm{i}}(k)}, \tag{2.8}$$

where $\hat{X}_{\mathrm{i}}(k)$ is the ith determined transmitted symbol, obtained from a demapping operation on $\hat{S}_{T,\mathrm{i}}(k)$ given from (2.7). Because the channel estimates in (2.8) are based on inherently unreliable data subcarriers, averaging in both frequency and time is employed to reduce the effects of noise and erroneous channel estimates caused by an incorrect determination of $\hat{X}_{\mathrm{i}}(k)$. First, averaging in frequency is performed as

$$\hat{H}_{\mathrm{STA,update}}(k) = \sum_{\lambda=-\beta}^{\lambda=\beta} \omega_\lambda \hat{H}'_{STA,\mathrm{i}}(k+\lambda), \tag{2.9}$$

where ω_λ is a set of weighting coefficients that sums unity, and β is an integer parameter that determinate how many subcarriers are averaged in the frequency domain. After this frequency averaging has been completed, the new channel estimate $\hat{H}_{STA,\mathrm{i}}(k)$ is computed as

$$\hat{H}_{STA,\mathrm{i}}(k) = \left(1 - \frac{1}{\alpha}\right) \hat{H}_{STA,\mathrm{i}-1}(k) + \frac{1}{\alpha} \hat{H}_{STA,\mathrm{update}}(k), \tag{2.10}$$

where α is an updating parameter. This channel estimate is used to equalize the next data symbol, and the process is repeated until the packet is completely demodulated. For comparison reasons, and for the reasons explained in [13], in this manuscript we use $\omega_\lambda = 1/(2\beta+1)$ and $\alpha = \beta = 2$, resulting in an average of 5 adjacent sub carriers in each channel estimation update. Note that if null carriers are adjacent, these are not considered and ω_λs are adjusted in order to sum unity. For example, if only 4 subcarriers are considered, as one of the original 5 subcarriers to be considered is null, ω_λ would be 1/4 instead of 1/5, as explained in [25].

2.4.3. Constructed Data Pilots Estimation

The CDP estimation is also based on the logic of the STA scheme, which dynamically updates the estimate of the channel, but it integrates the existing correlation between two consecutively transmitted symbols [4]. First, the estimates in (2.7) and (2.8) are done. Then, two equalization processes are performed as follows

$$\hat{S}'_{C,\mathrm{i}-1}(k) = \frac{Y_{R,\mathrm{i}-1}(k)}{\hat{H}'_{\mathrm{CDP,i}}(k)}, \tag{2.11}$$

$$\hat{S}''_{C,\mathrm{i}-1}(k) = \frac{Y_{R,\mathrm{i}-1}(k)}{\hat{H}_{\mathrm{CDP,i}-1}(k)}, \tag{2.12}$$

where $S_{R,\mathrm{i}-1}(k)$ is the previously demodulated received symbol. Whereas $\hat{H}'_{\mathrm{CDP,i}}(k)$ in (2.11) is obtained from (2.8), while $\hat{H}_{\mathrm{CDP,i}-1}$ is the previous channel estimate. To update the channel

estimate, a comparison process is performed. A demapping operation is performed both on (2.11) and (2.12), obtaining $\hat{X}'_{\mathrm{i}-1}(k)$ and $\hat{X}''_{\mathrm{i}-1}(k)$, respectively. As two time-adjacent received data symbols should have a high correlation on the channel response that both deal with it, if $\hat{X}'_{\mathrm{i}-1}(k) \neq \hat{X}''_{\mathrm{i}-1}(k)$, this implies that the demapping operation that gives $\hat{X}_{\mathrm{i}}(k)$, and subsequently $\hat{H}'_{\mathrm{CDP,i}}(k)$, is wrong. Hence, the update on the channel estimate is done by $\hat{H}_{\mathrm{CDP,i}}(k) = \hat{H}_{\mathrm{CDP,i}-1}$, i.e., the previous channel estimate is maintained on the kth subcarrier. If $\hat{X}'_{\mathrm{i}-1}(k) = \hat{X}''_{\mathrm{i}-1}(k)$, the channel estimate is updated as $\hat{H}_{\mathrm{CDP,i}}(k) = \hat{H}'_{\mathrm{CDP,i}}(k)$.

Again, the first data symbol of the package, $\hat{H}_{\mathrm{CDP,i}-1}$ corresponds to the LS estimation. It is clear from the previously described process that the updating on the channel estimate is done starting on the second symbol of the package. The first symbol of the package is equalized as it was done in (2.7).

Chapter 3

Mobile-to-Mobile Channel Model

Modelling the wireless propagation channel has been a constant challenge for the development of mobile radio communications technology. Whenever a good description of the impairments of the transmission medium is available, sets of countermeasures can be implemented on the communication systems. The impairments, or effects that the medium has on the transmitted signal, can be divided in two groups [26]:

- Large scale effects: These effects are considered when the communication link is established in distances that are much bigger than the wavelength of the transmitted signal.

- Small scale effects: These effects are considered when the communication link is established in distances that are only hundreds times the wavelength of the transmitted signal.

These groups of effects are statistically characterized. This is because, generally, there is no previous knowledge about the scenario where the communication process is taking place, and also, it is unknown how fast this scenario is changing.

Despite not having knowledge of the scenario where the communication is happening, through the literature, some assumptions are made for the channel modeling. One of these assumptions is the fact that the statistical properties of the communication channel are wide-sense stationary. However, the WSSUS assumption may not hold for some modern communication systems, which have been not previously studied by the literature. This would be the case of vehicular communications.

In the vehicular communications, not only the participants of the communications are moving, they are moving very fast. As a consequence, the propagation environment of communication is changing quickly. This new scenario for the communication systems presents many challenges. Among them, channel modeling is a very important one.

As it was stated before, a historical assumption for the wireless communication channels modeling, was the fact that the stochastic process that describes the channel was stationary. However, recent empirical evidence shows that this statistical assumption may not hold in

vehicular communication scenarios [6]. Despite the big amount of empirical evidence of this statistical characteristic of the vehicular channel, very few works have been made on the mathematical model of the effects of the vehicular environment.

To shade some light in this important subject, geometrical models of a mobile to mobile channel were developed in [8] and [9]. These works attempt to fully characterize the effects of a vehicular environment. Both works characterize the small scale effects, given that vehicular communications, generally, involve the transmission of data frames of a short duration, in the order of some few milliseconds. Having these effects characterized, these works derive expressions for a series of important statistical descriptors of the channel. Given the logic of the channel modeling, the resulting stochastic process is a non-stationary one, both in the time and frequency domain, meaning that the channel model does not fulfill the WSSUS condition.

The objective of the present chapter is to present the framework for the channel modeling that has been established in [8] and [9]. We pay special attention to the particular characteristics of the channel model that are relevant for this thesis. We study the statistics of particular propagation scenarios over which we will, in subsequent chapters, study the impact of the non-WSSUS condition on the BER performance.

3.1. Mathematical Model of Mobile to Mobile Channels

Given that vehicular communications are, generally, in short ranges, in this work we focus on the characterization of the small scale effects for time-frequency dispersive channels. To study them, the following transmission scenario is assumed: The signal of a transmitter antenna reaches a single receiver antenna, interacting only with $\mathcal{L}$ static interfering objects (IOs). The described scenario is shown in Fig. 3.1. In the Fig., the transmitter and the receiver are separated by a distance D, they are located at positions $\mathcal{O}$ and $\mathcal{O}'$, respectively, of the coordinate system defined in the x and y dimensions.

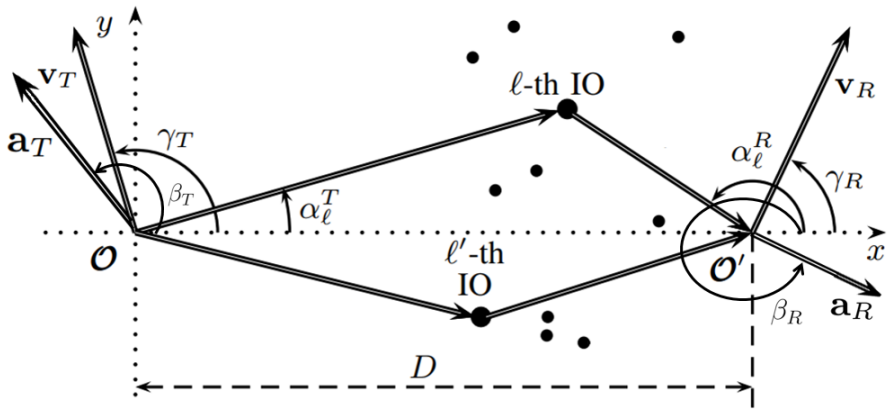

Figure 3.1: Transmission scenario.

Figure 3.1 illustrates the transmission of a signal that interacts with the ℓ and ℓ' IOs.

Parameters $\mathbf{v}_P$, $\mathbf{a}_P$, γ_P, β_P α_ℓ^P with $P \in \{T, R\}$ defines the following variables:

- $\mathbf{v}_P$ is the vector that describes the movement trajectory of the P mobile.
- $\mathbf{a}_P$ is the vector that describes the acceleration direction of the P mobile.
- γ_P is the angle in which is oriented $\mathbf{v}_P$ vector.
- β_P is the angle in which is oriented $\mathbf{a}_P$ vector.
- α_ℓ^P, for $P = T$, is the angle of departure (AOD) of the ℓ-th component of the transmitted signal.
- α_ℓ^P, for $P = R$, is the angle of arrival (AOA) of the ℓ-th component of the transmitted signal, after been scattered by the ℓ-th IO.

Because the parameters that define the multipath channel depend on unknown positions of an unknown number of IOs, it is convenient to statistically characterize the communication channel. To develop this characterization, we will first define the band pass $x_{BP}(t)$ equivalent of the transmitted signal $x(t)$

$$x_{BP}(t) = \Re\{x(t) \exp\{j2\pi f_c t\}\}, \tag{3.1}$$

where $\Re\{\cdot\}$ is the real part operator and f_c is the carrier frequency.

In the scenario described by Fig. 3.1, not taking in account the additive white gaussian noise (AWGN), the received signal is given by

$$y_{BP}(t) = \Re\left\{\sum_{\ell=1}^{\mathcal{L}(t)} g_\ell(t) \exp\{j\theta_\ell(t)\} x(t - \tau_\ell(t)) \exp\{j2\pi f_c (t - \tau_\ell(t))\}\right\}, \tag{3.2}$$

this is, the sum of the $\mathcal{L}(t)$ components of the signal, each one attenuated by a $g_\ell(t)$ factor, with a $\phi_\ell(t)$ phase shift and delayed by $\tau_\ell(t)$. Similar to (3.1), from (3.2) it is derived the complex base-band equivalent of the received signal, $y(t)$, given by

$$\begin{aligned} y(t) &= \sum_{\ell=1}^{\mathcal{L}(t)} g_\ell(t) \exp\{j(\theta_\ell(t) - 2\pi f_c \tau_\ell(t))\} x(t - \tau_\ell(t)), \\ &= x(t) * \sum_{\ell=1}^{\mathcal{L}(t)} g_\ell(t) \exp\{j(\theta_\ell(t) - 2\pi f_c \tau_\ell(t))\} \cdot \delta(t - \tau_\ell(t)), \end{aligned} \tag{3.3}$$

where $*$ is the convolution operator, and δ is the delta dirac function. the impulse response of the channel, $h(t, \tau)$, can be derived from (3.3), as follows,

$$h(t, \tau) \triangleq \sum_{\ell=1}^{\mathcal{L}(t)} g_\ell(t) \exp\{j(\theta_\ell(t) - 2\pi f_c \tau_\ell(t))\} \cdot \delta(t - \tau_\ell(t)). \tag{3.4}$$

In this way, the communication channel is defined as a system with input $x(t)$, output $y(t)$ and impulse response $h(t, \tau)$. Simplifying (3.2) we get

$$y(t) = \int h(\tau; t) x(t - \tau) \mathrm{d}\tau = x(t) * h(\tau, t). \tag{3.5}$$

To study the small scale fading, and to be able to characterize in a simple fashion the model of (3.4), an observation window T_0 small enough to ignore the effects of the large scale effects is assumed. Consequently, $t \in \{t_0, t_0+T_0\}$, where t_0 is the reference point where the observation window begins. It can be assumed that $t_0 = 0$ without loss of generality [8]. As a consequence, $h(\tau, t)$ is redefined as follows

$$h(\tau, t) = \sum_{\ell=1}^{\mathcal{L}(t)} g_\ell(t) \exp\{j(\theta_\ell(t) - 2\pi f_c \tau_\ell(t))\} \cdot \delta(t - \tau_\ell(t)) \cdot \Omega_{T_0}(t - t_0), \tag{3.6}$$

where $\Omega_{T_0}(t - t_0)$ is a windowing function defined as follows

$$\Omega_{T_0}(t - t_0) \triangleq \begin{cases} 1 & t_0 \leq t \leq t_0 + T_0 \\ 0 & \text{in other case.} \end{cases}$$

Considering a small time window T_0 also allows to neglect the time dependence of some of the components of the transmitted signal. First, it allows to redefine $\mathcal{L}(t)$ as $\mathcal{L}$. It also allows to neglect the temporal dependence of the variables $g_\ell(t)$ and $\theta_\ell(t)$, redefining them as g_ℓ and θ_ℓ, respectively. The values of these variables depend of the electromagnetic characteristics of the ℓ-th IO. However, on a real communication system, the electromagnetic characteristics of the objects that are present in the environment are not always known in advance. Literature show that real measured values of g_ℓ and θ_ℓ can be matched using random variables to model gains and phases [27]. So, using random variables allows to completely characterize the electromagnetic characteristics of objects that are commonly present in communication environment. Finally, $\tau_\ell(t)$ requires a more detailed explanation.

Most of the literature that deals with channel modeling assumes that the propagation environment is small enough to neglect the time dependence of the time delays $\tau_\ell(t)$. This assumptions is equivalent to saying that the mobiles involved in the communication are not moving fast enough. However, as literature and we have stated, this may not hold in vehicular environments. Having this clear, we characterize the time delays $\tau_\ell(t)$ considering their time dependence.

To characterize the propagation delays $\tau_\ell(t)$, these are defined as a linear function of time. This function describes the increment (or decrement) of the propagation delay, given an initial delay and a function that characterize the trajectory of the mobiles, in both the dimension of the movement and the acceleration.

$$\tau_\ell(t) = \tau_\ell(t_0) - \tau_{t,\ell}(t). \tag{3.7}$$

In Fig. 3.1, we will define the initial distance between the transmitter and the ℓ-th IO as d_ℓ^T. Also, we will define the initial distance between the ℓ-th IO and the receiver as d_ℓ^R. Thus, the initial delay of the ℓ-th trajectory of the signal, $\tau_\ell(t_0)$ in (3.7), is given by

$$\tau_\ell(t_0) = \frac{\mathrm{d}_\ell^T + \mathrm{d}_\ell^R}{\mathcal{C}}, \tag{3.8}$$

where $\mathcal{C}$ is the speed of the light. The function $\tau_{t,\ell}(t)$ that describes the delay given the

trajectory of the mobiles is given by

$$\tau_{t,\ell}(t) = t\Bigg[\frac{v_T}{\mathcal{C}}\cos(\alpha_\ell^T(t)-\gamma_T) + \frac{v_R}{\mathcal{C}}\cos(\alpha_\ell^R(t)-\gamma_R) + \frac{1}{2}\left(\frac{a_T t}{\mathcal{C}}\cos(\alpha_\ell^T(t)-\beta_T) + \frac{a_R t}{\mathcal{C}}\cos(\alpha_\ell^R(t)-\beta_R)\right)\Bigg]$$
$$= t\Bigg[\frac{f_{\max}^T}{f_c}\cos(\alpha_\ell^T(t)-\gamma_T) + \frac{f_{\max}^R}{f_c}\cos(\alpha_\ell^R(t)-\gamma_R) + \frac{1}{2}\left(\frac{\dot{f}_{\max}^T(t)}{f_c}\cos(\alpha_\ell^T(t)-\beta_T) + \frac{\dot{f}_{\max}^R(t)}{f_c}\cos(\alpha_\ell^R(t)-\beta_R)\right)\Bigg]$$
$$= \frac{t}{f_c}\Bigg[f_{\max}^T\cos(\alpha_\ell^T(t)-\gamma_T) + f_{\max}^R\cos(\alpha_\ell^R(t)-\gamma_R) + \frac{1}{2}\left(\dot{f}_{\max}^T(t)\cos(\alpha_\ell^T(t)-\beta_T) + \dot{f}_{\max}^R(t)\cos(\alpha_\ell^R(t)-\beta_R)\right)\Bigg], \quad (3.9)$$

where $f_{\max}^P = \mathbf{v}_P/\lambda$ and $\dot{f}_{\max}^P(t) = \mathbf{a}_P \cdot t/\lambda$ for $P \in \{T, R\}$, where λ stands for the wavelength of the transmitted signal. Also, v_P and a_P are the scalar values of the vectors that describe the velocity and the acceleration trajectories in Fig. 3.1, respectively. Finally, we got,

$$\tau_{t,\ell}(t) = \frac{t}{f_c}\left[f_\ell^S + \frac{\dot{f}_\ell^A(t)}{2}\right], \quad (3.10)$$

where f_ℓ^S and $\dot{f}_\ell^A(t)$ are defined as follows,

$$f_\ell^S = f_{\max}^T\cos(\alpha_\ell^T(t)-\gamma_T) + f_{\max}^R\cos(\alpha_\ell^R(t)-\gamma_R), \quad (3.11)$$

$$\dot{f}_\ell^A(t) = \dot{f}_{\max}^T(t)\cos(\alpha_\ell^T(t)-\beta_T) + \dot{f}_{\max}^R(t)\cos(\alpha_\ell^R(t)-\beta_R). \quad (3.12)$$

Both $f_{\max}^P$ and $\dot{f}_{\max}^P(t)$ characterize the maximum Doppler shift caused by the speed and acceleration of the mobiles, respectively [9], [28]. Thus, $\tau_{t,\ell}(t)$ in (3.10) characterize the increment (or decrement) of the propagation delay given the accelerated motion of the mobiles, for the communication channel defined in (3.4) and (3.6).

Having completely defined the time dependent delays, it is of interest to this thesis to model some statistics of the channel model defined in (3.6). However, given that the propagation environment is unknown (there is no a priori knowledge about the distribution of the IOs), and also the fact that it is constantly changing, the variables $\alpha_\ell^T(t)$ should be modeled as random processes. As a consequence, the characterization of the channel defined in (3.6) becomes a very though task. As we assume that far field conditions are met, the AOD and AOA are no longer dependent on time [29], redefining $\alpha_\ell^P(t)$ as α_ℓ^P for $P \in \{T, R\}$.

With all the parameters of the channel model of (3.6) characterized, we redefined it, along with the propagation delays, as follows

$$h(\tau, t) = \sum_{\ell=1}^{\mathcal{L}} g_\ell \exp\{j(\theta_\ell - 2\pi f_c \tau_\ell(t))\} \cdot \delta(t - \tau_\ell(t)) \cdot \Omega_{T_0}(t - t_0), \quad (3.13)$$

$$\tau_\ell(t) = \frac{\mathrm{d}_\ell^T + \mathrm{d}_\ell^R}{\mathcal{C}} - \frac{t}{f_c}\left[f_\ell^S + \frac{\dot{f}_\ell^A(t)}{2}\right], \tag{3.14}$$

$$f_\ell^S = f_{\max}^T \cos(\alpha_\ell^T - \gamma_T) + f_{\max}^R \cos(\alpha_\ell^R - \gamma_R), \tag{3.15}$$

$$\dot{f}_\ell^A(t) = \dot{f}_{\max}^T(t) \cos(\alpha_\ell^T - \beta_T) + \dot{f}_{\max}^R(t) \cos(\alpha_\ell^R - \beta_R). \tag{3.16}$$

Through (3.13) to (3.16), g_ℓ, θ_ℓ and α_ℓ^P are defined as random variables.

Finally, to study its statistical properties, we define the time-frequency varying transfer function of the channel $h(\tau, t)$, $H(t, f)$ as

$$\begin{aligned} H(t,f) &\triangleq \int_{-\infty}^{\infty} h(\tau,t)\mathrm{e}^{-j2\pi f\tau}\mathrm{d}\tau \\ &= \Omega_{T_0}(t-t_0)\int_{-\infty}^{\infty}\sum_{\ell=1}^{\mathcal{L}} g_\ell \exp\{j(\theta_\ell - 2\pi f_c\tau_\ell(t))\}\exp\{-j2\pi f\tau\}\delta(\tau-\tau_\ell(t))\mathrm{d}\tau \\ &= \Omega_{T_0}(t-t_0)\sum_{\ell=1}^{\mathcal{L}} g_\ell \exp\{j(\theta_\ell - 2\pi\tau_\ell(t)[f_c+f])\}. \end{aligned} \tag{3.17}$$

3.2. Statistical Characterization of the Channel Model

3.2.1. Considerations

In [8] and [9] several statistics of the channel model defined in (3.17) are studied. However, for this thesis, we put our focus in the correlation function. To study the correlation function the following considerations are taken on the random variables

- The mean value of the gains of the paths of the signal are given as follows

$$\sum_{\ell=1}^{\mathcal{L}} \mathcal{E}\{|g_\ell|^2\} = \sigma_h^2,$$

  where $\mathcal{E}\{\cdot\}$ is the expected value operator.
- As is common in the literature, the phase shifts of each θ_ℓ are uniformly distributed in $[-\pi, \pi]$ [26].
- The characterization of the AOA are quite complex without a prior knowledge of the propagation scenario. This subject will be studied in a subsequence section.

3.2.2. Four Dimensional Time Frequency Correlation Function

Been characterize the random variables of the transfer function defined in (3.17), in this section we study the Four Dimensional Time Frequency Correlation Function (4D TF-CF),

defined here as in [30]

$$\mathcal{R}_H(t,f;\Delta t,\Delta f) \triangleq \mathcal{E}\{H^*(t-\Delta t,f)H(t,f+\Delta f)\}, \tag{3.18}$$

where $(\cdot)^*$ is the complex conjugate operator. Assuming $t_0 = 0$, here we work out (3.18).

$$H^*(t-\Delta t,f) = \Omega_{T_0}(t-\Delta t)\sum_{\ell=1}^{\mathcal{L}} g_\ell \exp\{-j(\theta_\ell - 2\pi\tau_\ell(t-\Delta t)[f_c+f])\}$$

$$= \Omega_{T_0}(t-\Delta t)\sum_{\ell=1}^{\mathcal{L}} g_\ell \exp\{-j(\theta_\ell - 2\pi\left(\frac{\mathrm{d}_\ell^T+\mathrm{d}_\ell^R}{\mathcal{C}} - t\left[f_\ell^S + \frac{\dot{f}_\ell^A(t)}{2}\right] + \Delta t\left[f_\ell^S + \frac{\dot{f}_\ell^A(t)}{2}\right]\right)[f_c+f])\}.$$

Similarly,

$$H(t,f+\Delta f) = \Omega_{T_0}(t)\sum_{\ell=1}^{\mathcal{L}} g_\ell \exp\{j(\theta_\ell - 2\pi\tau_\ell(t)[f_c+f+\Delta f])\}$$

$$= \Omega_{T_0}(t)\sum_{\ell=1}^{\mathcal{L}} g_\ell \exp\{j(\theta_\ell - 2\pi\left(\frac{\mathrm{d}_\ell^T+\mathrm{d}_\ell^R}{\mathcal{C}} - t\left[f_\ell^S + \frac{\dot{f}_\ell^A(t)}{2}\right]\right)[f_c+f+\Delta f])\}.$$

Finally,

$$H^*(t-\Delta t,f)H(t,f+\Delta f) = \Omega_{T_0}(t)\Omega_{T_0}(t-\Delta t)\cdot$$
$$\sum_{\ell=1}^{\mathcal{L}} g_\ell^2 \exp\left\{2\pi j\left[\Delta t\left[f_\ell^S + \frac{\dot{f}_\ell^A(t)}{2}\right]\left(\frac{f_c+f}{f_c}\right) + \Delta f\left(\frac{t}{f_c}\left[f_\ell^S + \frac{\dot{f}_\ell^A(t)}{2}\right] - \frac{\mathrm{d}_\ell^T+\mathrm{d}_\ell^R}{\mathcal{C}}\right)\right]\right\}.$$

When the expected value is applied to this last equation, the random variable g_ℓ is independent to the random variable of the exponential. In this way, the expected value of the product factors is the product of the expected values. In the argument of the exponential function, the only random variable is given by the function that characterizes the Doppler effect, defined in (3.10). In (3.10), the random variable is given by the AOD or the AOA. This is because it is assumed that the interaction with the IOs occurs on only one side of the communication. Thus, the other angle can be calculated as a function of the random variable selected. For this case, we will assume that the interactions happens at the receiver side of the communications. Consequentely, the AOA α_ℓ^R is a random variable, and the AOD α_ℓ^T can be calculated as a function of the AOA. If the distribution of α_ℓ^R is given by $p_\alpha^R(\alpha)$, the 4D TF-CF is given by

$$\mathcal{R}_H(t,f;\Delta t,\Delta f) = \sigma_h^2\Omega_{T_0}(t)\Omega_{T_0}(t-\Delta t)\cdot$$
$$\int_{-\pi}^{\pi} p_\alpha^R(\alpha)\exp\left\{2\pi j\left[\Delta t\left[f_\ell^S + \frac{\dot{f}_\ell^A(t)}{2}\right]\left(\frac{f_c+f}{f_c}\right) + \Delta f\left(\frac{t}{f_c}\left[f_\ell^S + \frac{\dot{f}_\ell^A(t)}{2}\right] - \frac{\mathrm{d}^T+\mathrm{d}^R}{\mathcal{C}}\right)\right]\right\}\mathrm{d}\alpha. \tag{3.19}$$

3.2.3. Wide sense stationary analysis

A stochastic process is said to be wide sense stationary (or weakyl stationary) if the following two conditions are met [31]:

- Mean value should be invariant in the analysis domain.
- The correlation function of the process should only depend on the shifts around the origin in the domain of analysis, and not to the specifics points of the domain that is been analyzed.

The second condition establishes that necessarily

$$\mathcal{R}_H(t_\mathrm{i}, f_\mathrm{i}; \Delta t, \Delta f) = \mathcal{R}_H(t_k, f_k; \Delta t, \Delta f),$$

for all i $\neq k$, Δt, $\Delta f \in \mathbb{R}$. If (3.19) is analyzed, it can be seen that in the arguments of the integral exists dependence both on frequency and time. Thus, when the integral is solved, respect to the AOA, it is not possible to eliminate the time and frequency domain. This turns the stochastic process induced by the channel $H(t, f)$ in a non-stationary process, both on time and frequency domain.

3.3. Single Ring Geometrical Model

In [8], an approximation that allows a simplification of the transmission scenario is proposed. In this approximation, it is assumed that the IOs are circularly distributed, within a ratio d, surrounding the side of the communication where they are located. Figure 3.2 illustrates this approximation. Through this approximation, a closed form for the integral of the

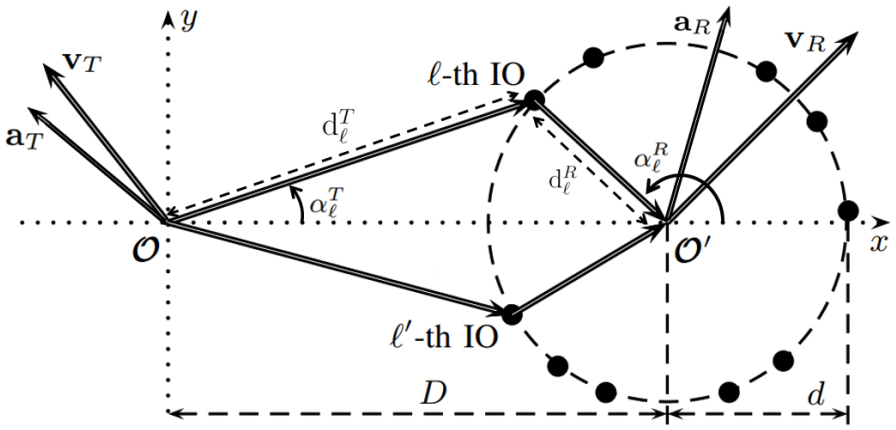

Figure 3.2: Single Ring Geometrical Model surrounding the receiver Agregar vector de aceleración.

4D TF-CF defined in (3.19) can be found. For that purpose, it is assumed that the AOAs follow a von Mises distribution with mean value $\mu \in [-\pi, \pi)$ and concentration parameter κ, $0 \leq \kappa \leq \infty$. Thus,

$$p_\alpha^R(\alpha) = \frac{\exp\{\kappa \cos(\alpha - \mu)\}}{2\pi I_0(\kappa)} \tag{3.20}$$

with $\alpha \in [-\pi, \pi)$. In (3.20), $I_0(\cdot)$ the modified Bessel Function of the first kind and zero order.

The use of the von Misses distribution to model AOA of an scenario as is shown if Fig. 3.2 was proposed in [32]. In this article, the authors show evidence that the von Misses distribution fits with a series of empirical measurement data. This model has been widely used for other types of wireless channels.

3.3.1. Relation between AOD and AOA

Lets define $\alpha_\ell'^R$ as the complementary angle to α_ℓ^R in Fig. 3.2. If $\mathrm{d}_{x,\ell}^R$ is the x component of the distance d_ℓ^R, we have

$$\cos(\alpha_\ell'^R) = \frac{\mathrm{d}_{\ell,x}^R}{\mathrm{d}_\ell^R} \implies \mathrm{d}_{\ell,x}^R = \mathrm{d}_\ell^R \cos(\alpha_\ell'^R).$$

If $\mathrm{d}_{x,\ell}^T$ is the x component of the distance d_ℓ^T, we have

$$\mathrm{d}_{x,\ell}^T = D - \mathrm{d}_{x,\ell}^R = D - \mathrm{d}_\ell^R \cos(\alpha_\ell'^R),$$

thus, the cosine of the AOD is given by

$$\cos(\alpha_\ell^T) = \frac{D - \mathrm{d}_\ell^R \cos(\alpha_\ell'^R)}{\mathrm{d}_\ell^T} = \frac{D + \mathrm{d}_\ell^R \cos(\alpha_\ell^R)}{\mathrm{d}_\ell^T}.$$

Finally,

$$\alpha_\ell^T = \cos^{-1}\left(\frac{D + \mathrm{d}_\ell^R \cos(\alpha_\ell^R)}{\mathrm{d}_\ell^T}\right), \tag{3.21}$$

where α_ℓ^R follows the distribution defined in (3.20).

3.3.2. Four Dimensional Time Frequency Correlation Function for the Geometrical Single Ring Model

In [9] is shown that if $\mathrm{d} << D$, using the von Misses distribution and the Equation $(3{,}338-4)$ of [33], the 4D TF-CF can be approximated as

$$\mathcal{R}_H(t,f;\Delta t,\Delta f) = \sigma_h^2 \Omega_{T_0}(t)\Omega_{T_0}(t-\Delta t) \times \frac{\exp\{j2\pi\mathcal{A}(t,f;\Delta t,\Delta f)\}}{I_0(\kappa)} \times$$
$$I_0\left(\left\{[\kappa\cos(\mu) - j2\pi\mathcal{B}_c(t,f;\Delta t,\Delta f)]^2 + [\kappa\sin(\mu) - j2\pi\mathcal{B}_s(t,f;\Delta t,\Delta f)]^2\right\}^{1/2}\right), \tag{3.22}$$

$$\mathcal{A}(t,f;\Delta t,\Delta f) = \mathcal{Z}(t,f;\Delta t,\Delta f)F_c^T(t) + \mathcal{W}(t,f,\Delta t)\dot{f}_{\max}^T(\Delta t)\cos(\beta_T) - \Delta f\left(\frac{D+\mathrm{d}}{\mathcal{C}}\right), \tag{3.23}$$

$$\mathcal{B}_c(t,f;\Delta t,\Delta f) = \mathcal{Z}(t,f;\Delta t,\Delta f)F_c^R(t) + \mathcal{W}(t,f,\Delta t)\dot{f}_{\max}^R(\Delta t)\cos(\beta_R) - \Delta f\frac{\mathrm{d}}{\mathcal{C}}, \tag{3.24}$$

$$\mathcal{B}_s(t,f;\Delta t,\Delta f) = \mathcal{Z}(t,f;\Delta t,\Delta f)\left[\frac{\mathrm{d}}{D}F_s^T(t) + F_s^R(t)\right] + \mathcal{W}(t,f,\Delta t)\left[\frac{\mathrm{d}}{D}\dot{f}^T_{\max}(\Delta t)\sin(\beta_T) + \dot{f}^R_{\max}(\Delta t)\sin(\beta_R)\right]. \quad (3.25)$$

Finally, functions $\mathcal{Z}(t,f;\Delta t,\Delta f)$, $\mathcal{W}(t,f,\Delta t)$, $F_c^P(t)$, and $F_s^P(t)$ are given by:

$$\mathcal{Z}(t,f;\Delta t,\Delta f) = \Delta t\left(\frac{f_c+f}{f_c}\right) + \Delta f\frac{t}{f_c}, \quad (3.26)$$

$$\mathcal{W}(t,f,\Delta t) = \left(\frac{t-\Delta t}{2}\right)\left(\frac{f_c+f}{f_c}\right), \quad (3.27)$$

$$F_c^P(t) = f^P_{\max}\cos(\gamma_P) + \frac{\dot{f}^P_{\max}(t)}{2}\cos(\beta_P), \quad (3.28)$$

$$F_s^P(t) = f^P_{\max}\sin(\gamma_P) + \frac{\dot{f}^P_{\max}(t)}{2}\sin(\beta_P), \quad (3.29)$$

for $P \in \{T,R\}$.

3.3.3. Numerical Results

To illustrate the non-stationary behaviour of the correlation function, we performed simulations using the parameters of the Table 3.1. The parameters of bandwidth and carrier frequency corresponds to the one established on the IEEE 802.11p protocol for vehicular communications. Over this protocol, an observation window of $T_0 = 6{,}4$ ms corresponds to the transmission of 1000 symbols.

Table 3.1: Simulation parameters.

Parameter	**Value**
Channel mean power	$\sigma_h^2 = 1$
Carrier frequency	$f_c = 5,9$ GHz
Bandwidth	$B = 10$ MHz
Observation window time Ω_{T_0}	$T_0 = 6{,}4$ ms
Transmitter velocity	$v_T = 40$ km/h
Receiver velocity	$v_R = 40$ km/h
Transmitter acceleration	$a_T = 10$ m/s^2
Receiver acceleration	$a_R = 10$ m/s^2
Transmitter movement angle	$\gamma_T = 105°$
Receiver movement angle	$\gamma_R = 70°$
Transmitter acceleration angle	$\beta_T = 105°$
Receiver acceleration angle	$\gamma_R = 250°$
Initial distance between the transmitter and the receiver	$D = 300$ m
Radius of the ring of IOs	d = 30 m

For this work, it is assumed that the propagation scenario is a non-isotropic one. This condition establishes that the signal does not has a preference path for its propagation.

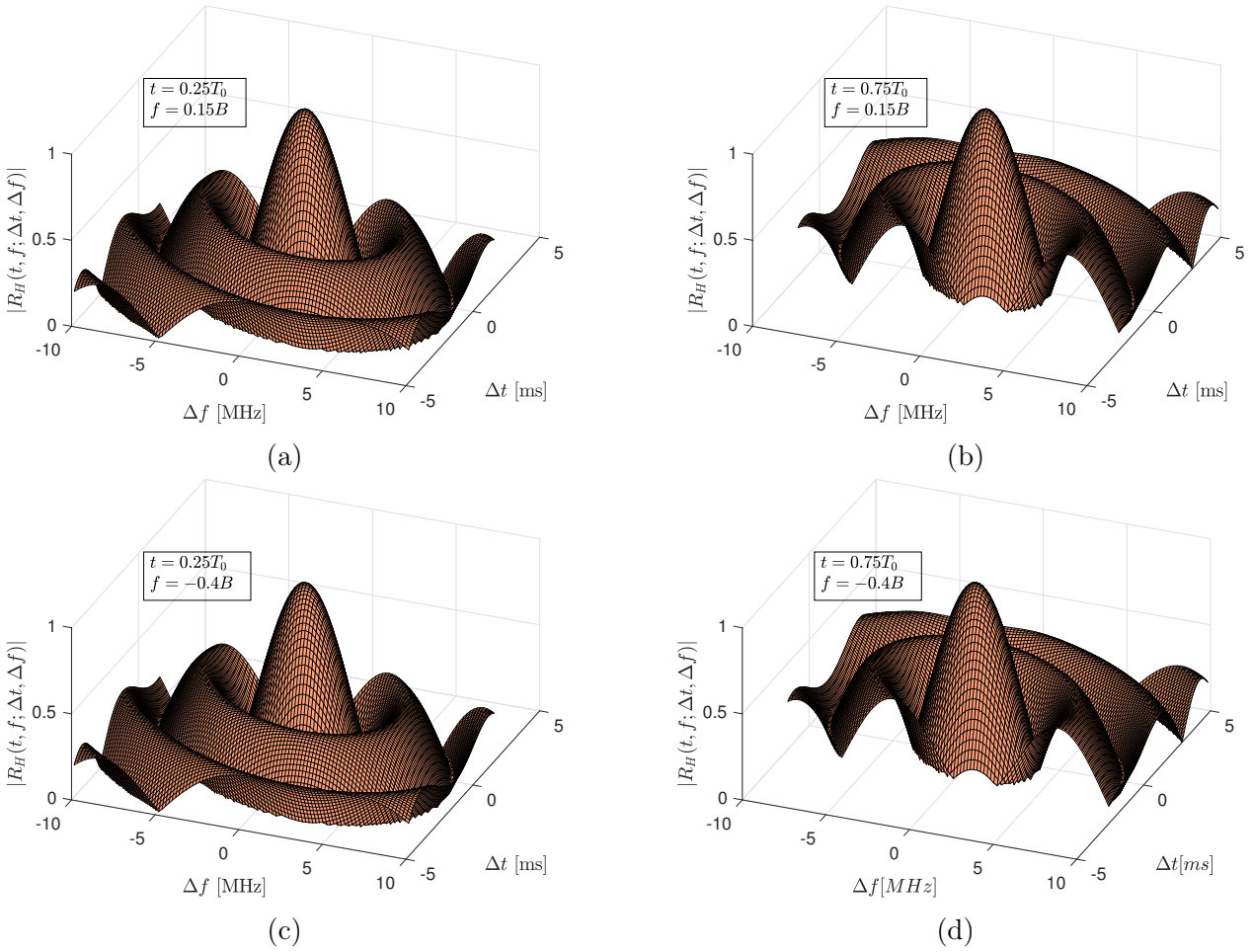

Figure 3.3: Absolute value of the 4D TF-CF $\mathcal{R}_H(t, f; \Delta t, \Delta f)$ in four points of the observation domain.

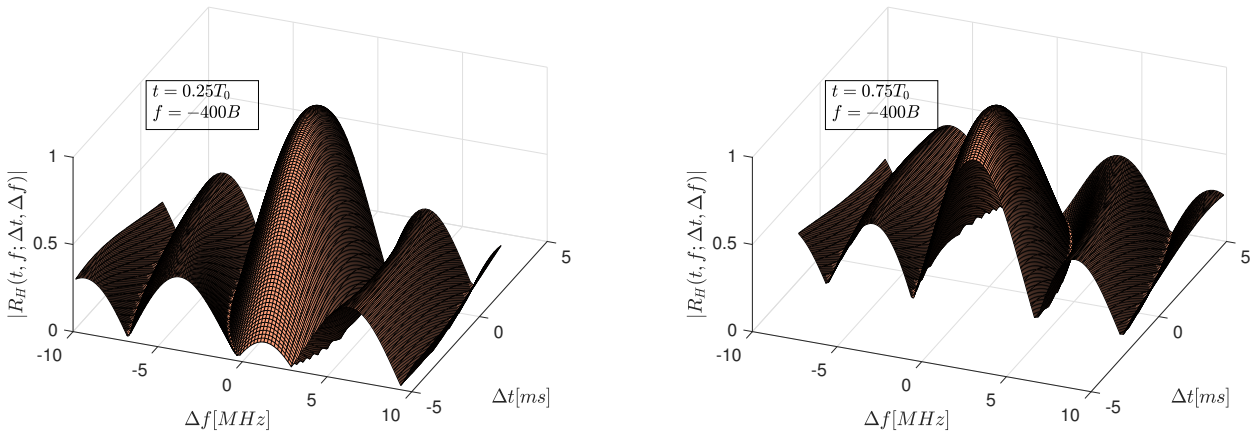

(a) (b)

Figure 3.4: Absolute value of the 4D TF-CF $\mathcal{R}_H(t, f; \Delta t, \Delta f)$ in two points of the observation domain.

Under this consideration, the von Misses distribution defined in (3.20) has a concentration parameter $\kappa = 0$. Thus, p_α^R distribution is reduced to a uniform distribution $U[-\pi, \pi]$. Finally, the domain of the correlation function $\mathcal{R}_H(t, f; \Delta t, \Delta f)$ is defined in $t \in [0, T_0]$, $\Delta t \in [t - T_0, t]$, $f \in [-B/2, B/2]$ and $\Delta f \in [-B, B]$.

Figure 3.3 shows the behaviour of the correlation function in four points of the domain. As it was established in section 3.2.3, the correlation function generally defined in (3.19) describes a non-stationary process both on the time and frequency domain. This can bee seen in Figures 3.3a and 3.3b. These two Figures shows that the correlation function changes for two instants of observation, not fulfilling, in the time domain, the second condition established in section 3.2.3. The same point can be established when Figures 3.3c and 3.3d are compared.

To analyze the non-stationarities of the frequency domain, Figures 3.3a and 3.3c must be compared. From these Figures it can be seen that there is no major changes in the correlation function if we observe the instants $f = 0{,}15B$ and $f = -0{,}4B$. We can see the same if we compare Figures 3.3b and 3.3d. This may lead to the conclusion that, despite the existence of an explicit dependence of f in (3.19), the process may be stationary in the frequency domain. However, if the observation point in the frequency domain is much farther, the non-stationarities can be clearly seen. This is shown in Fig. 3.4, where the observation point in the frequency domain is $f = -400B$. It can be seen, comparing Figures 3.3a and 3.3c with Fig. 3.4a, that the correlation function varies when a fixed time $t = 0{,}25T_0$ is studied in two far enough frequency points. The same can be concluded observing Figures 3.3b and 3.3d and comparing them to Fig. 3.4b, on the time instant $t = 0{,}75T_0$. From these comparisons we have shown that the process that describes the channel, under the conditions established, is also non-stationary in the frequency domain. However, these non-stationarities in the frequency domain, are less severe that the ones that can be seen in the time domain.

The non-stationarities, in both domains, can also be seen in the lack of symmetry of $|\mathcal{R}_H(t, f; \Delta t, \Delta f)|$. As is established in [31], an stationary stochastic process possesses Hermitian symmetry. We will illustrate the existence or absence of symmetry in both domains in Figures 3.5 and 3.6.

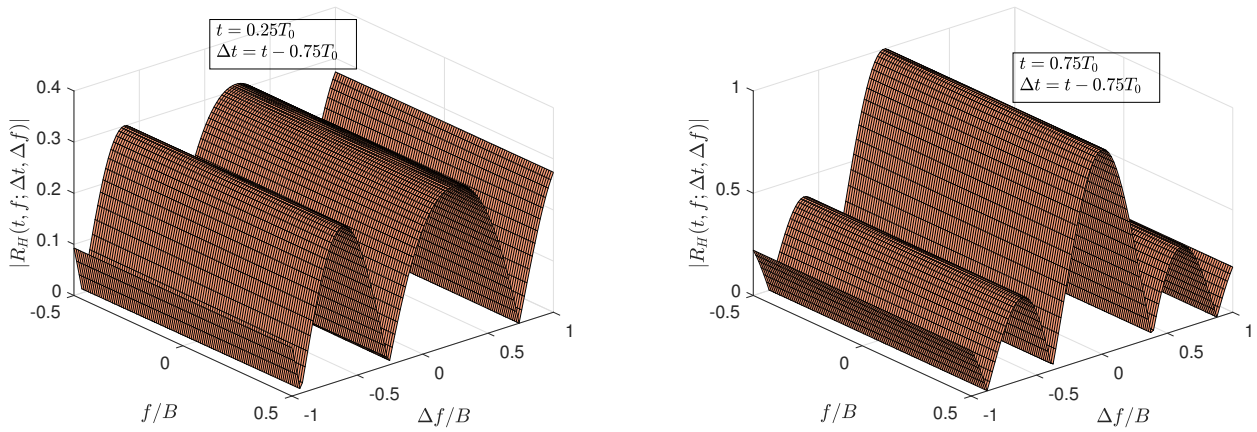

(a) (b)

Figure 3.5: Absolute value of the 4D TF-CF $\mathcal{R}_H(t, f; \Delta t, \Delta f)$ in two points of the observation domain.

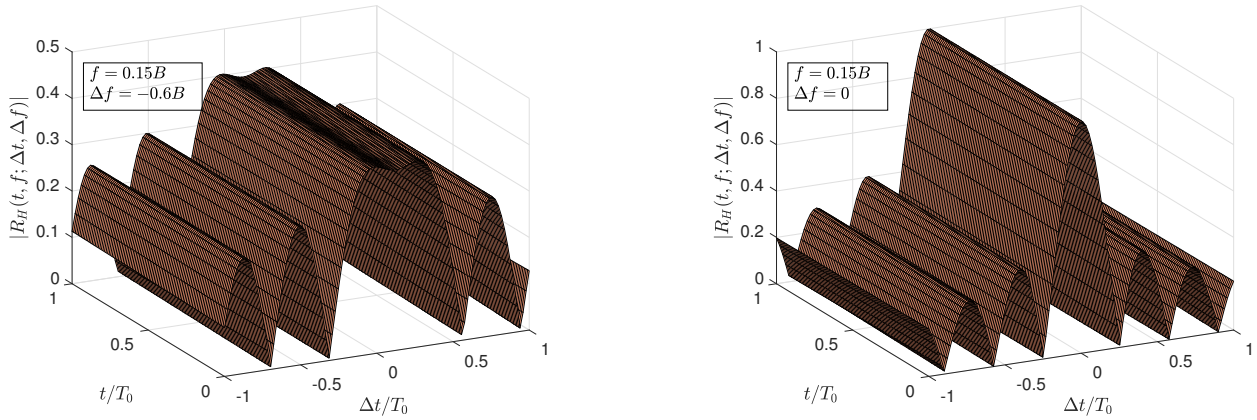

(a) (b)

Figure 3.6: Absolute value of the 4D TF-CF $\mathcal{R}_H(t, f; \Delta t, \Delta f)$ in two points of the observation domain.

In Fig. 3.5, the axes have been changed with respect to Fig. 3.3. For this analysis, points t and Δt are fixed and variations on f/B and $\Delta f/B$ are analyzed. In Fig. 3.5a is seen a clear asymmetry round $\Delta f/B = 0$ in the correlation function. However, if the analysis point is coincident with Δt equal to zero, as in Fig. 3.5b, the correlation function is symmetric with respect to $\Delta f/B$. This result is consistent with the fact that if we got a closer look to Equations (3.22) to (3.29), making $\Delta t = 0$, the frequency dependence of the correlation function is neglected. As a consequence, the process becomes stationary in the frequency domain.

Finally, observing Fig. 3.6, it is seen that something very similar to Fig. 3.5 happens, but in the time domain. In Fig. 3.6, we can see a clear asymmetry round de origin $\Delta t/T_0 = 0$. If the observation point Δf is equal to 0, the correlation becomes clearly symmetrical, as it seen in Fig. 3.6b. Again, if we study Equations (3.22) to (3.29), when we make $\Delta f = 0$, the dependence with respect to t is eliminated, turning the stochastic process in a stationary one in the time domain.

Chapter 4

Doppler Shift Characterization of Wideband Mobile Radio Channels

Given the non-stationarities of the channel model presented in the previous Chapter, we now put our attention in the definition of the Doppler Shift (DS) for wideband channels. We present an expression for the Doppler that is time and frequency dependent. From this definition, we found the origins of the non-stationarities that was evidenced in Chapter 3. We perform a series of experiments that allow to observe the variations on the ratio of decorrelation in different frequencies. This chapter is based on the material presented in [15].

4.1. The Doppler Shift from a Time-Frequency Analysis Perspective

4.1.1. Doppler Shift for Narrowband Signals

We first analyze the case of an unmodulated carrier of frequency f_c, which is transmitted over a single-path mobile radio channel. For this case, the DS can be modeled from a time-frequency (TF) analysis perspective [34] as

$$f_D(t) = \frac{1}{2\pi}\frac{\mathrm{d}}{\mathrm{d}t}[\arg\{y_{BP}(t)\} - \arg\{x_{BP}(t)\}]. \tag{4.1}$$

Equation (4.1) states that the DS is given by the difference of the Instantaneous Frequency (IF) of the received signal minus the IF of the transmitted signal [34]. The DS is modeled in (4.1) as a time-varying quantity because the IF of $y_{BP}(t)$ changes in time if the transmitter, the receiver, or the scatterers (or a combination thereof) move with a constant or time-varying velocity [35], or if the angular statistics of the received signal vary in time [8], [36]. However, the DS can be characterized as a time-invariant quantity if the channel's angular statistics an the velocities of the aforementioned wandering elements do not change over time.

From the theory of linear time-varying (LTV) systems [37], the received signal $y_{BP}(t)$ is

given by

$$y_{BP}(t) = H_{BP}(t; f) \exp\{j2\pi ft\}|_{f=f_c}, \tag{4.2}$$

for the case of a signal transmitted in a single path mobile radio channel. In (4.2), H_{BP} is the band pass equivalent of the Channel Transfer Function (CTF). For the case of a single path mobile radio channel we have $x_{BP}(t) = \exp\{j2\pi f_c t\}$. Evaluating $x_{BP}(t)$ and (4.2) in (4.1) we have

$$f_D(t) = \frac{1}{2\pi}\frac{\mathrm{d}}{\mathrm{d}t}\arg\{H_{BP}(t; f)\}|_{f=f_c}. \tag{4.3}$$

If we analyze the low pass equivalent defined in Chapter 3 for the CTF, we have

$$f_D(t) = \frac{1}{2\pi}\frac{\mathrm{d}}{\mathrm{d}t}\arg\{H(t; f)\}|_{f=0}. \tag{4.4}$$

If we now consider the transmission of $x_{BP}(t)$ over a mobile radio channel comprising $\mathcal{L}$ different propagation paths, the received signal can be modeled as

$$y_{BP}(t) = \sum_{\ell=1}^{\mathcal{L}} y_{BP,\ell}(t), \tag{4.5}$$

where $y_{BP,\ell}(t)$ is the signal that arrives at the receiver through the ℓ-th propagation path. According to the definition of the IF of a multicomponent signal [34], a single DS has to be computed for each component of $y_{BP}(t)$. Following a similar procedure as in (4.4), the DS of the ℓ-th component of $y_{BP}(t)$ is equal to

$$f_{D,\ell}(t) = \frac{1}{2\pi}\frac{\mathrm{d}}{\mathrm{d}t}\arg\{H_\ell(t; f)\}|_{f=0}. \tag{4.6}$$

where $H_\ell(t; f)$ denotes the complex baseband CTF associated with the ℓ-th propagation path, for $\ell \in \{1, 2, \ldots, \mathcal{L}\}$. Equation 4.6 shows that the DS of narrowband mobile radio channels is given by the IF of the channel's complex envelope. This DS model is equivalent to that proposed in [35] for the characterization of non-stationary M2M channels under non-uniform motion of the transmitter and the receiver. This narrowband description of $f_{D,\ell}(t)$ is equivalent to the one obtained from differentation of the received carrier's phase [26].

4.1.2. Doppler Shift Characterization for Wideband Signals

Now we analyze the case of an arbitrary band-limited signal $x_{BP}(t)$ transmitted over a single-path channel. From the theory of LTV systems [37] we have

$$x_{BP}(t) \approx \frac{1}{2\pi}\int_{f_c-B/2}^{f_c+B/2} X_{BP}(f) \exp\{j2\pi ft\}\mathrm{d}f, \tag{4.7}$$

$$y_{BP}(t) \approx \frac{1}{2\pi}\int_{f_c-B/2}^{f_c+B/2} H_{BP}(t; f)X_{BP}(f) \exp\{j2\pi ft\}\mathrm{d}f, \tag{4.8}$$

where $X_{BP}(f)$ is the fourier transform of $x_{BP}(t)$ and B is the signal's bandwidth. For this analysis, we establish that $f_c > B/2$. Integrals in (4.7) and (4.8) can be approximated by a Riemann sum consisting in N terms as

$$x_{BP}(t) = \frac{1}{2\pi}\sum_{n=1}^{N} X_{BP}(\xi + n\Delta)\exp\{j2\pi(\xi + n\Delta)t\}\Delta, \tag{4.9}$$

$$y_{BP}(t) = \frac{1}{2\pi}\sum_{n=1}^{N} H_{BP}(t;\xi + n\Delta)X_{BP}(\xi + n\Delta)\exp\{j2\pi(\xi + n\Delta)t\}\Delta, \tag{4.10}$$

where $\Delta = B/N$ and $\xi = f_c - B/2$. Note that such approximations are defined with respect to the same partition of the integration interval, and they converge to $x_{BP}(t)$ and $y_{BP}(t)$ in the limit if $N \to \infty$. Equations (4.9) and (4.10) show that $x_{BP}(t)$ and $y_{BP}(t)$ are multicomponent signals. Thus, the DS for these signals should be computed individually for each element of the series. Similar to the discussion on the previous section, the DS of the n-th spectral component of $y_{BP}(t)$ is given by

$$f_{D,n}(t) = \frac{1}{2\pi}\frac{\mathrm{d}}{\mathrm{d}t}[\arg\{y_{n,BP}(t) - x_{n,BP}(t)\}], \tag{4.11}$$

where $x_{n,BP}(t)$ and $y_{n,BP}(t)$ are given by

$$x_{n,BP}(t) = \frac{\Delta}{2\pi}X_{BP}(\xi + n\Delta)\exp\{j2\pi(\xi + n\Delta)t\}, \tag{4.12}$$

$$y_{n,BP}(t) = H_{n,BP}(t;\xi + n\Delta)\frac{\Delta}{2\pi}X_{BP}(\xi + n\Delta)\exp\{j2\pi(\xi + n\Delta)t\}. \tag{4.13}$$

Evaluating (4.12) and (4.13) in (4.11) we have

$$f_{D,n}(t) = \frac{1}{2\pi}\frac{\mathrm{d}}{\mathrm{d}t}\arg\{H_{BP}(t;\xi + n\Delta)\}, \tag{4.14}$$

for $n = 1, 2, \ldots, N$. In the limit, as $N \to \infty$ (and $\Delta \to 0$), the countably set of Doppler frequencies $\{f_{D,n}(t)\}_{n=1}^{N}$ can be modeled by a non-countably set $\{f_D(t;f') \in \mathbb{R}\}$ where

$$f_D(t;f') = \frac{1}{2\pi}\frac{\mathrm{d}}{\mathrm{d}t}\arg\{H_{BP}(t;f)\}|_{f=f_c+f'}, \tag{4.15}$$

with $t \in \mathbb{R}$ and $f' \in [-B/2, B/2]$. Expressing (4.15) in terms of the low pass equivalent of the CTF, we have

$$f_D(t;f) = \frac{1}{2\pi}\frac{\mathrm{d}}{\mathrm{d}t}\arg\{H(t;f)\}, \;\; |f| \leq B/2. \tag{4.16}$$

Similarly to subsection 4.1.1, in the extension of (4.4) to (4.6), if the signal propagates in $\mathcal{L}$ paths, the DS of the ℓ-th component of the received wideband multipath signal can be written as

$$f_{D,\ell}(t;f) = \frac{1}{2\pi}\frac{\mathrm{d}}{\mathrm{d}t}\arg\{H_\ell(t;f)\}, \;\; |f| \leq B/2. \tag{4.17}$$

There is a subtle difference when comparing (4.16) and (4.17) to (4.4) and (4.6), respectively, but it is worth to mention. We present (4.4) and (4.6) as particular cases of (4.16) and (4.17), where the narrowband characteristic of the transmitted signal has suppressed the frequency dependent of the DS defined in (4.4) and (4.6).

4.1.3. On the Frequency Dependence of the Doppler Shift

Equation 4.17 shows that the DS of wideband channels varies in both time and frequency. The time-varying character of $f_D(t;f)$ is only recently acknowledged within the field of land mobile radio communications [35], [36]. The DS's frequency dependence, on the other hand, remains largely unknown. Here we need to remind the definition of the CTF defined in Chapter 3

$$H(t;f) = \sum_{\ell=1}^{\mathcal{L}} g_\ell \exp\{-j[\theta_\ell + 2\pi\tau_\ell(t)(f_c+f)]\}. \tag{4.18}$$

By substituting (4.18) into (4.17) we find

$$f_{D,\ell}(t;f) = -(f_c+f)\frac{\mathrm{d}\tau_\ell(t)}{\mathrm{d}t}, \tag{4.19}$$

for $f \in [-B/2, B/2]$. This latter equation is noteworthy, as it not only shows that the DS is a frequency-dependent quantity, it also states that the DS and the propagation delay are related to each other in such way that $f_{D,\ell}(t;f)$ can be determined directly form $\tau_\ell(t)$. In turn, $\tau_\ell(t)$ can be computed from $f_{D,\ell}(t;f)$ provided that the initial conditions of the system are known, such tat

$$\tau_\ell(t) = \tau_\ell^0 - \frac{1}{f_c+f}\int_0^t f_{D,\ell}(x;f)\mathrm{d}x, \tag{4.20}$$

where τ_ℓ^0 is the initial propagation delay of the ℓ-th multipath component of $H(t;f)$. These two fundamental relationships between $f_D(t;f)$ and $\tau_\ell)(t)$ are often left aside assuming that the channel's Doppler and delay statistics are separable, or that the DSs are different from zero and the propagation delays are time invariant.

4.2. Influence of the Frequency-Varying DS on the Channel's Non-Stationary Characteristics

Even though the DS's frequency dependence has passed nearly unnoticed in the field of land mobile radio communications, this feature of $f_D(t;f)$ is widely acknowledged in other of the telecommunications, such as in underwater acoustic communications [38]. However, several questions remain open, such as those pertaining to the effects that the frequency-varying character of $f_D(t;f)$ has on the channel's statistical properties.

The origin of the DS's frequency-varying character is explained by observing that the maximum DS (MDS) $f_{\max}$ of a monochromatic signal is proportional to the signal's frequency f according to the well-known relation $f_{\max} = fv/c$ [26]. Hence, for a wideband signal, having spectral components whose frequencies span an interval $f_c - B/2 < f < f_c + B/2$, the MDS is a monotonically increasing linear function of f given by

$$f_{\max} = f_{\max}^0 \gamma(f) \tag{4.21}$$

where $f_{\max}^0 = f_c v/c$ is the carreier signal's MDS, and $\gamma(f)$ is a proportionally factor equal to

$$\gamma(f) = \frac{f_c + f}{f_c}, \ f \in [-B/2, B/2] \tag{4.22}$$

The frequency dependence of $f_{\max}(f)$ produces faster fades for the signal's spectral components of higher frequencies. We now illustrate this latter fact with some experiments.

Figures 4.1 to 4.4 illustrate the absolute value of (4.18). As in Chapter 3, this simulations are carried out with $\mathcal{L} = 20$, the gains g_ℓ are modeled by independent and identically distributed random variables characterized by a Rayleigh distribution, whereas the phases θ_ℓ are modeled as independent and identically distributed random variables uniformly distributed in $[\pi, \pi)$. The time delays are defined as in Chapter 3. In Figures 4.1 to 4.4, $f_c = 5{,}9$ GHz and B is the bandwidth of the transmitted signal. We consider, for the four Figures, an observation time interval of length $T_0 = 19{,}2$ ms, corresponding to the transmission of 3000 symbols on the IEEE 802.11p standard. Table 4.1 specifies the parameters for the simulation of Fig. 4.1.

Table 4.1: Simulation Parameters for Fig. 4.1.

Parameter	**Value**
Bandwidth	2 GHz
Transmitter velocity	$v_T = 40$ km/h
Receiver velocity	$v_R = 40$ km/h
Transmitter acceleration	$a_T = 0$ m/s^2
Receiver acceleration	$a_R = 0$ m/s^2
Transmitter movement angle	$\gamma_T = 60°$
Receiver movement angle	$\gamma_R = 120°$
Transmitter acceleration angle	$\beta_T = 0°$
Receiver acceleration angle	$\gamma_R = 0°$
Initial distance between the transmitter and the receiver	$D = 500$ m
Radius of the ring of IOs	d = 30 m

Table 4.1 specifies a scenario where two vehicles are moving, at constant velocities, on two perpendicular streets that intersect at one point. The use of a bandwidth of 2 GHz is for illustration purposes, as the effects of the non-stationarities can be seen for a big enough bandwidth. The analysis of this scenario is interesting, as it allows us to evidence the effect of the non-stationarities. If we study narrow-band cases, it could be wrongly concluded that the non-stationarities are not present.

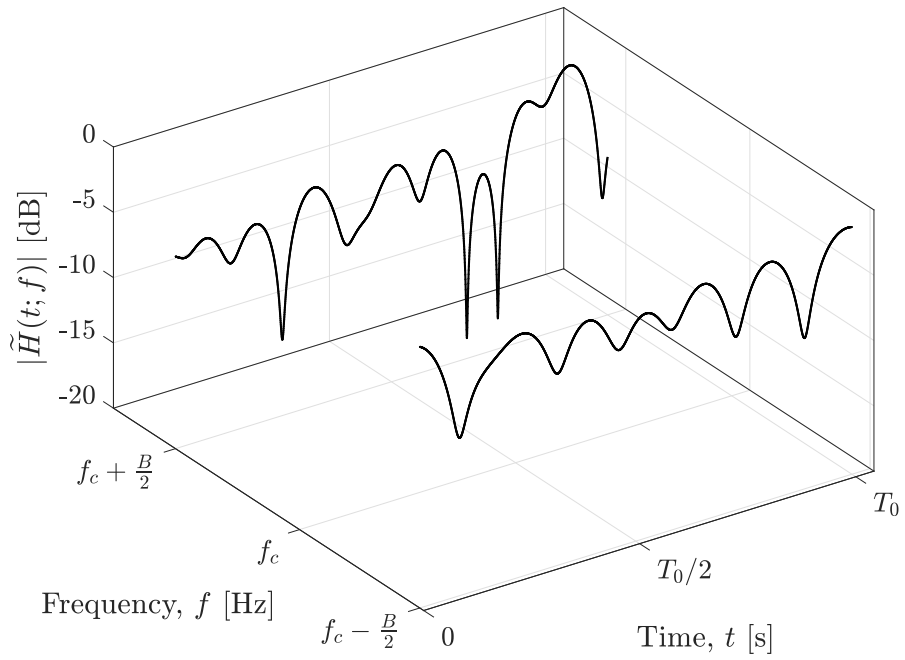

Figure 4.1: Absolute value of the Channel Transfer Function, given the parameters of Table 4.1.

Figure 4.1 shows that the waveform of higher frequency $f_2 = f_c + B/2$ varies faster than the waveform of lower frequency $f_2 = f_c - B/2$. These differences in fading rate cause the second order statistics of $H(t; f)$ to be jointly non-stationary in time and frequency, because the waveforms of higher frequencies decorrelate faster than those of lower frequencies. We now put our attention in an scenario on the framework of the IEEE 802.11p.

Table 4.2: Simulation parameters for Fig. 4.2.

Parameter	**Value**
Bandwidth	10 MHz
Transmitter velocity	$v_T = 40$ km/h
Receiver velocity	$v_R = 40$ km/h
Transmitter acceleration	$a_T = 0$ m/s^2
Receiver acceleration	$a_R = 0$ m/s^2
Transmitter movement angle	$\gamma_T = 60°$
Receiver movement angle	$\gamma_R = 120°$
Transmitter acceleration angle	$\beta_T = 0°$
Receiver acceleration angle	$\gamma_R = 0°$
Initial distance between the transmitter and the receiver	$D = 500$ m
Radius of the ring of IOs	d = 30 m

Table 4.2 specifies the same scenario, in terms of velocity and movement, as in 4.1. However, here we use a bandwidth of 10 MHz as it is specified in the IEEE 802.11p standard.

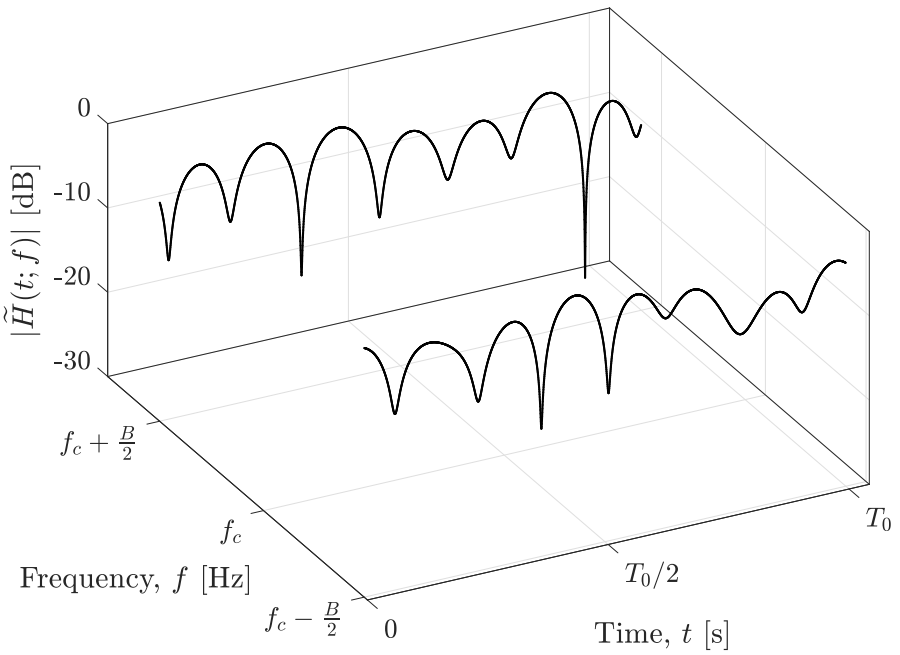

Figure 4.2: Absolute value of the Channel Transfer Function, given the parameters of Table 4.2.

Figure 4.2 show much more similar fading patterns, in comparison to Fig. 4.1, for frequencies $f_c - B/2$ and $f_c + B/2$. This is the scenario to be expected if we give a look to (4.21), as a extreme frequencies has a lower distance between them. Nonetheless these findings, if the movement parameters varies, the behaviour of the fadings rates may vary. We inspect those cases in Figures 4.3 and 4.4.

Table 4.3: Simulation parameters for Fig. 4.3.

Parameter	**Value**
Bandwidth	2 GHz
Transmitter velocity	$v_T = 40$ km/h
Receiver velocity	$v_R = 40$ km/h
Transmitter acceleration	$a_T = 10$ m/s^2
Receiver acceleration	$a_R = 10$ m/s^2
Transmitter movement angle	$\gamma_T = 60°$
Receiver movement angle	$\gamma_R = 120°$
Transmitter acceleration angle	$\beta_T = 60°$
Receiver acceleration angle	$\gamma_R = 300°$
Initial distance between the transmitter and the receiver	$D = 500$ m
Radius of the ring of IOs	d = 30 m

Table 4.3 specifies an scenario where two vehicles are moving on two perpendicular streets that intersect at one point. However, here we incorporate changing in the velocities of the

mobiles, as the transmitter is accelerating and the receiver is decelerating. Again, the use of a bandwidth of 2 GHz is for illustration purposes.

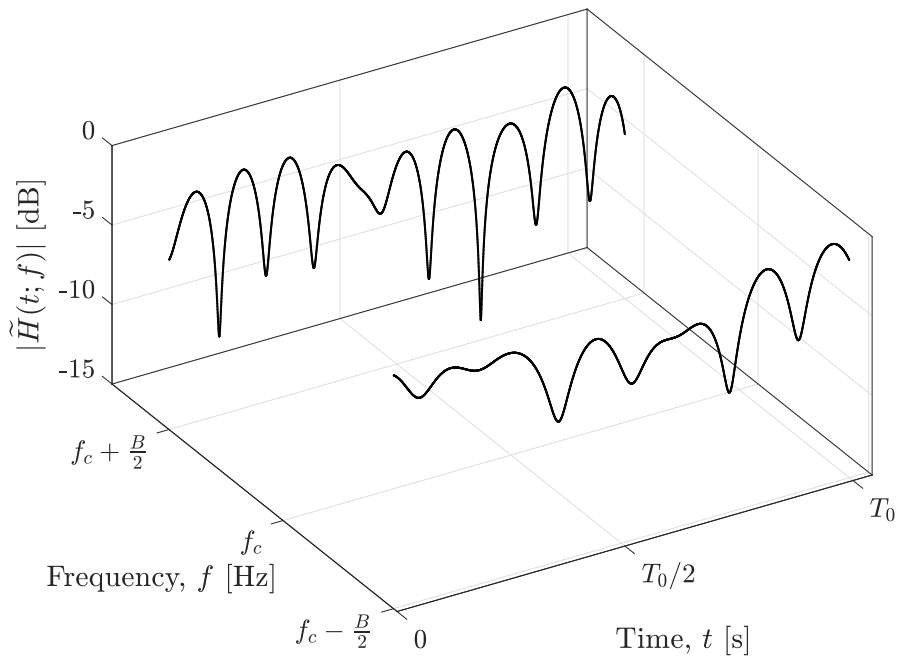

Figure 4.3: Absolute value of the Channel Transfer Function, given the parameters of Table 4.3.

Figure 4.3 shows that the waveform of higher frequency $f_2 = f_c + B/2$ varies faster than the waveform of lower frequency $f_2 = f_c - B/2$, as it also was seen in Fig. 4.1. We can elaborate the same reasons for this behaviour as the ones stated in Fig 4.1. We now study this scenario on the framework of the IEEE 802.11p protocol.

Table 4.4: Simulation parameters for Fig. 4.4.

Parameter	**Value**
Bandwidth	10 MHz
Transmitter velocity	$v_T = 40$ km/h
Receiver velocity	$v_R = 40$ km/h
Transmitter acceleration	$a_T = 10$ m/s^2
Receiver acceleration	$a_R = 10$ m/s^2
Transmitter movement angle	$\gamma_T = 60°$
Receiver movement angle	$\gamma_R = 120°$
Transmitter acceleration angle	$\beta_T = 60°$
Receiver acceleration angle	$\gamma_R = 300°$
Initial distance between the transmitter and the receiver	$D = 500$ m
Radius of the ring of IOs	d = 30 m

Table 4.4 specifies the same scenario, in terms of velocity and movement, as in 4.3. Howe-

ver, here we use a bandwidth of 10 MHz as it is specified in the IEEE 802.11p standard.

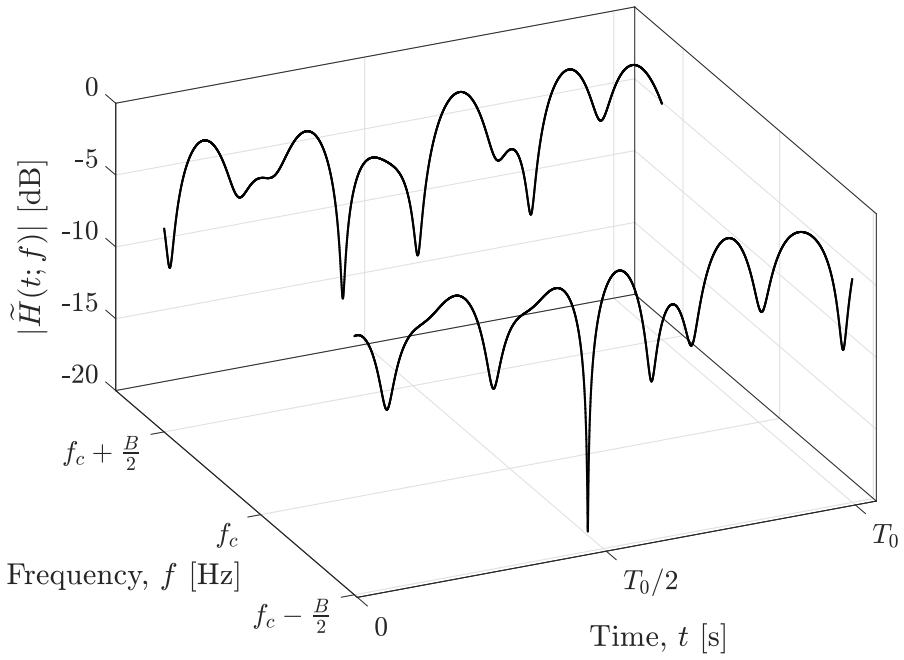

Figure 4.4: Absolute value of the Channel Transfer Function, given the parameters of Table 4.4.

Figure 4.3 show much more similar fading patterns, in comparison to Fig. 4.4, for frequencies $f_c - B/2$ and $f_c + B/2$. This behaviour is the same that when Figures 4.1 and 4.2 are compared. As a initial conclusion, we can state that the velocities variations that the mobiles may have, do not affect the behaviour of the transfer function. Nonetheless this latter fact, particular effects on the system performance of this velocity variations are studied in Chapter 5.

Chapter 5

Results and Discussion

As we have established in Chapter 3, a vehicular communication channel, given some particular conditions, presents strong non-stationarities, both in the time and the frequency domain. Moreover, we established in Chapter 4 that the main cause of the non-stationarities is the Doppler effect. In Chapter 4 we have characterized the Doppler effect for wide-band communication channels in a general manner. This generalized characterization can be used to study the vehicular communications environments that are been studied in this work. With the concepts and origins of the non-stationarities completely clear, we now perform some numerical experiments to see the effects of the non-stationarities in the system's performance.

The main objective of this chapter is to study the effects of the non-stationarities on the BER performance of an IEEE 802.11p communication system. We divide our study into two parts. The first one compares the performance of the channel estimation techniques described in chapter 2 in two different channel models, a WSSUS one, and the non-WSSUS model described in [8]. The model presented in [8] is for fixed velocity mobiles. The second part of our study uses the model presented in [9]. This model allows us to simulate velocity changes, i.e., accelerated motion into the mobiles. We use this model to inspect the effect on the BER performance of the system when some parameters associated with the Doppler effect are changed, namely, the distance between the mobiles, and their speeds and accelerations. We also study some specific points of the correlation function presented in Chapter 3 to see how the second-order statistics are changed when we vary the aforementioned parameters.

5.1. Stationary and non-Stationary Comparison

To compare the performance of an IEEE 802.11p communication system under a WSSUS model and a non-WSSUS model, we simulate a unidirectional single user communication between two mobile stations. To obtain the BER performances of the LS, STA and CPD estimators, we perform Monte Carlo simulations. Table 5.1 defines the parameters for the simulations. As it has been stated, vehicular communications' main application is road safety. For that reason, the speed and acceleration angle parameters that are given in Table 5.1 describe a scenario where the receiver is decelerating, while the transmitter is accelerating and

Table 5.1: Simulation parameters.

Parameter	**Value**
Channel mean power	$\sigma_h^2 = 1$
Carrier frequency	$f_c = 5{,}9$ GHz
Bandwidth	$B = 10$ MHz
Modulation	BPSK
Transmitter velocity	$v_T = 40$ km/h
Receiver velocity	$v_R = 40$ km/h
Receiver movement angle	$\gamma_R = 70°$
Transmitter acceleration angle	$\beta_T = 105°$
Receiver acceleration angle	$\gamma_R = 250°$
Initial distance between the transmitter and the receiver	$D = 300$ m
Radius of the ring of IOs	d = 30 m

changing lanes in preparation to overtake the receiver. The rest of the parameters correspond to the specifications of the IEEE 802.11p, except for the selected number of symbols on a package.

Figures 5.1 to 5.3 shows the BER performance of the LS, STA and CDP estimators, respectively. Their performance are compared under a WSSUS scenario and a non-WSSUS scenario. Figures 5.1 and 5.3 show that time-domain based estimators, i.e., the estimation is only based on previously sent OFDM symbols, are not quite affected by the non-stationarities. We can see a slight difference on the performance of the LS estimator, been the WSSUS case the one where this estimator achieves the best performance. On the other side, Fig. 5.2 shows something radically different for the STA estimator, which is a time and frequency-domain estimator, i.e., its estimation take in account the previously sent OFDM symbol and also the estimation on adjacent sub-carriers. Figure 5.2 shows that the STA estimator radically improves its performance on the stationary case. This result indicates that the linear averaging process performed on the STA estimator drastically degrades the performance of the estimator on the non-stationary case (a highly frequency selective channel). Finally, we can see in Fig. 5.3 that the CDP channel estimator (a time-domain technique) is not affected by the non-stationarities, achieving exactly the same performance on both WSSUS and non-WSSUS cases.

Finally, in Fig. 5.4 we show a performance comparison between the three estimators when they are used in the non-WSSUS model. As Figures 5.1 to 5.3 have shown, the LS estimator and the CDP are not influenced by the non-stationarities in their BER performance. It can be seen that for low E_b/N_0 regimes, the LS estimator is the one who has the best performance. Nonetheless, the BER values where the LS estimator achieves the best performance are not acceptable, been the BER higher than 0,1. As the E_b/N_0 increases, the STA and the CDP estimators achieve performances that considerably outperform the LS estimator, being the CDP estimator the one who obtains the better BER performance. When the BER downs to 0,01, the CDP estimator outperforms the other two channel estimation techniques by far.

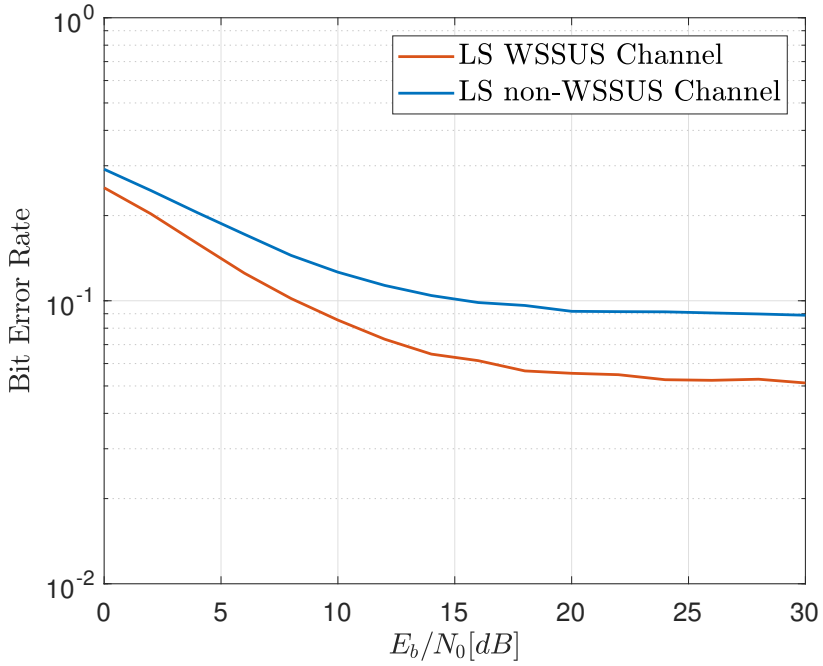

Figure 5.1: BER performance of the LS estimator under two channel models.

5.2. Doppler Parameter Comparison on the non-Stationary Model

In this sub-section, we perform two numerical experiments to analyze the behavior of the 4D TF-CF defined in Chapter 3. We simulate a unidirectional single user communication between two mobile stations. In the first experiment, we analyze the 4D TF-CF behavior changing the acceleration of both the transmitter and the receiver, a_T and a_R, respectively. For the second experiment, we vary the initial distance D between the transmitter and the receiver to see how the 4D TF-CF changes. We also perform Monte Carlo simulations to obtain the BER performances of the LS, STA and CP estimators on both experiments scenarios. Table 5.2 defines the common parameters for the simulations. Speed and acceleration angle parameters that are given in Table 5.2 describes the same scenario that Table 5.1.

Figure 5.5 shows the behavior of the 4D TF-CF on two different observation points, for two different acceleration values for the transmitter and the receiver. The domain of $\mathcal{R}_H$ is defined for $t \in \{0, T_0\}$, $\Delta t \in \{-T_0, T_0\}$, $f \in \{-B/2, B/2\}$ and $\Delta f \in \{-B, B\}$. The figure shows a frequency-domain non-stationary process on the two observation points. The non-stationarities can be seen, as the absolute value of $\mathcal{R}_H$ is clearly asymmetric with respect to the origin, and does not reach its maximum of $\Delta f = 0$. The conditions for stationarity are violated on both of the acceleration values evaluated for the transmitter and the receiver. Even though the process is non-stationary in the frequency domain, Fig. 5.5 shows that the second order statistics of the process does not change if acceleration increases. Second-order statistics behavior impacts on the BER performance of the system can be seen in Figures 5.6 to 5.8.

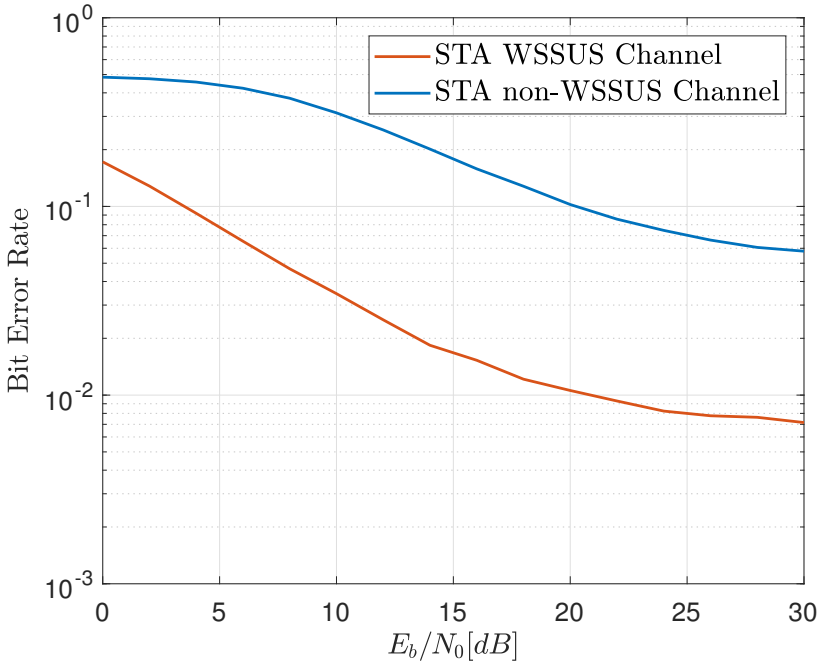

Figure 5.2: BER performance of the STA estimator under two channel models.

Figures 5.6 to 5.8 shows the BER performance for the LS, STA and CDP estimators. The three channel estimation techniques are evaluated for the same acceleration values as in Fig. 5.5. Figures 5.6 to 5.8 show that accelerations have no impact on the BER performance of the LS, STA and CDP estimators.

Figures 5.5 to 5.8 may lead to the conclusion that the non-stationarities, caused by the accelerated motion of the mobiles incorporated on the channel model, have no impact on the BER performance of the system. However, there are some other parameters that can be evaluated in order to gain more insights on how the second-order statistics of the channel behaves, and how this behavior affects the system overall performance. In Figures 5.9 to 5.12 we study the effect of changing the initial distance.

Figure 5.9 shows the behavior of the 4D TF-CF on two different observation points, for two different initial distance values. The domain of $\mathcal{R}_H$ is the same as in Fig. 5.5. Similarly to Fig. 5.5, Fig. 5.9 shows a frequency-domain non-stationary process on the observations points. However, here we can see some slight differences in the second-order statistics of the process when the initial distance of the transmission changes. Differences between the processes for different distances can be more clearly seen on Δt_1 observation point. These little changes on the second-order statistics have a considerable impact on the system's BER performance, as it can be seen in Figures 5.10 to 5.12.

Figures 5.10 to 5.12 show the BER performance for the LS, STA and CDP estimators. The three channel estimation techniques are evaluated for the same initial distance values as in Fig. 5.9. Despite the little changes seen on the second-order statistics in Fig. 5.9, Fig. 5.11 shows a considerable impact on the BER performance of the STA estimator. On the other hand, Figures 5.10 and 5.12 show that there is no impact on the BER performance of the LS

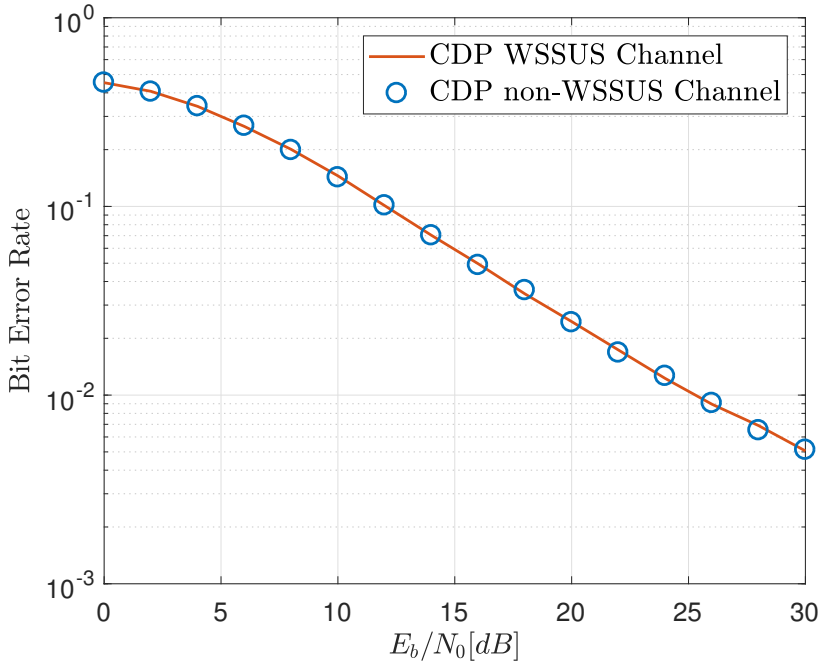

Figure 5.3: BER performance of the CDP estimator under two channel models.

and CDP estimators.

The fact that the initial distance between the transmitter and the receiver affects BER performance of the system is interesting, as the channel model defined in Chapter 3 does not consider large scale effects. As a consequence, this degradation on the BER performance is only produced by Doppler effect caused the motion of the mobiles.

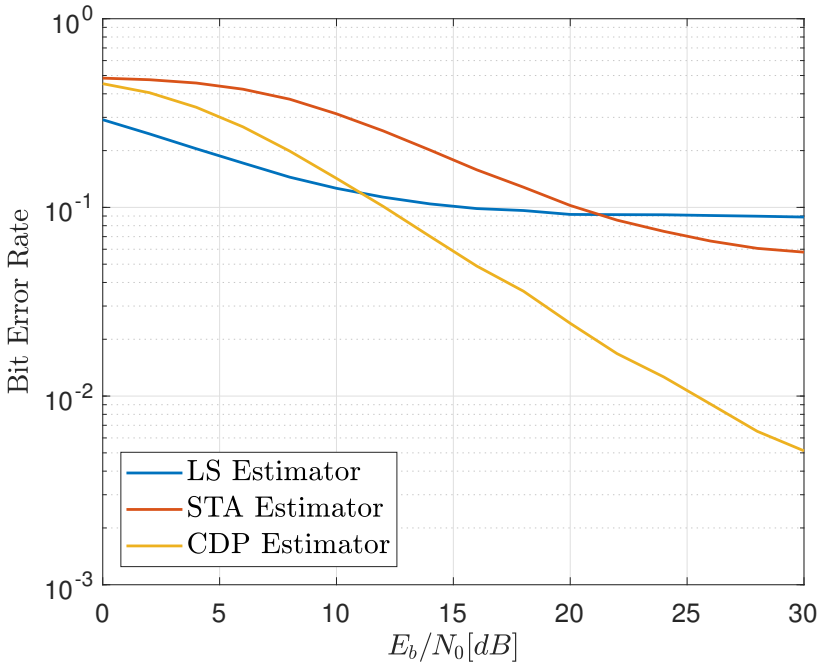

Figure 5.4: BER performance of the LS, STA, and CDP estimator under the non-WSSUS channel model.

Table 5.2: Common simulation parameters.

Parameter	**Value**
Carrier frequency	$f_c = 5{,}9$ GHz
Bandwidth	$B = 10$ MHz
Modulation	BPSK
Number of OFDM symbols per package	128
Observation window length Ω_{T_0}	$T_0 = 1$ ms
Radius of the scattering ring	d = 30 m
Velocities	$v_T = v_R = 40$ km/h
Transmitter movement angle	$\gamma_T = 105°$
Receiver movement angle	$\gamma_R = 70°$
Transmitter acceleration angle	$\beta_T = 105°$
Receiver acceleration angle	$\beta_R = 250°$

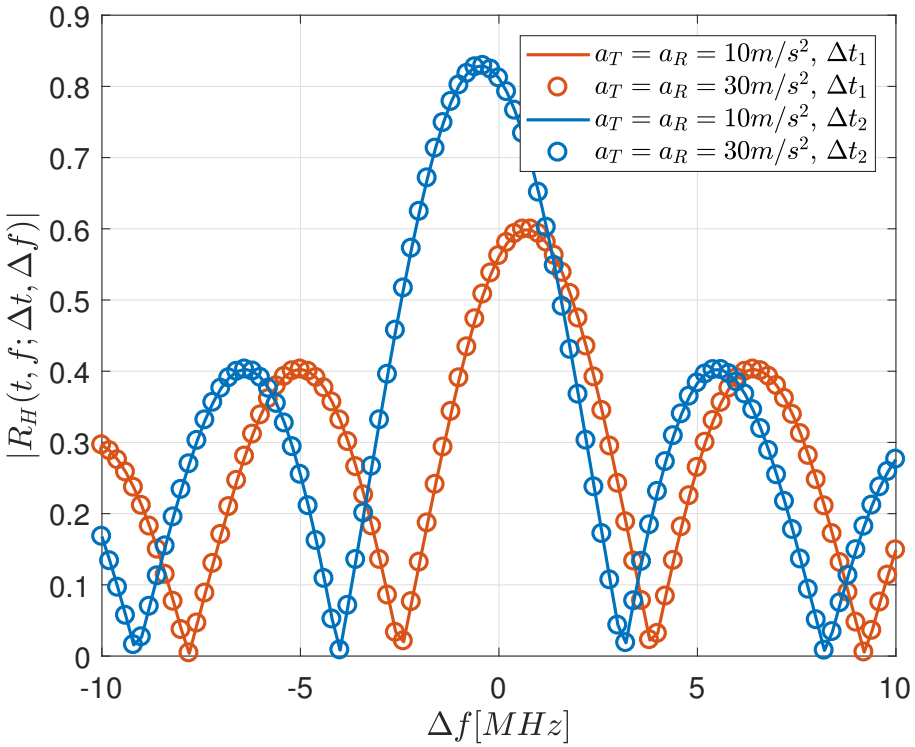

Figure 5.5: 4D TF-CF for observation points ($t = 0{,}5T_0$, $f = 0{,}25B$, $\Delta t_1 = -0{,}92T_0$) and ($t = 0{,}5T_0$, $f = 0{,}25B$, $\Delta t_2 = 0{,}58T_0$). $D = 300$ m for both acceleration values.

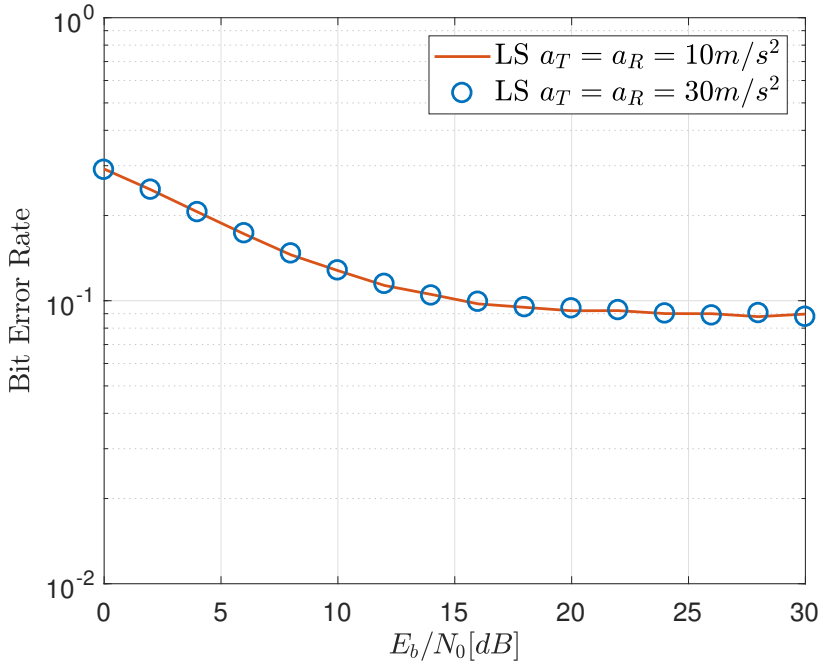

Figure 5.6: BER performance for the LS estimator, for different acceleration values. $D = 300$ m on both curves.

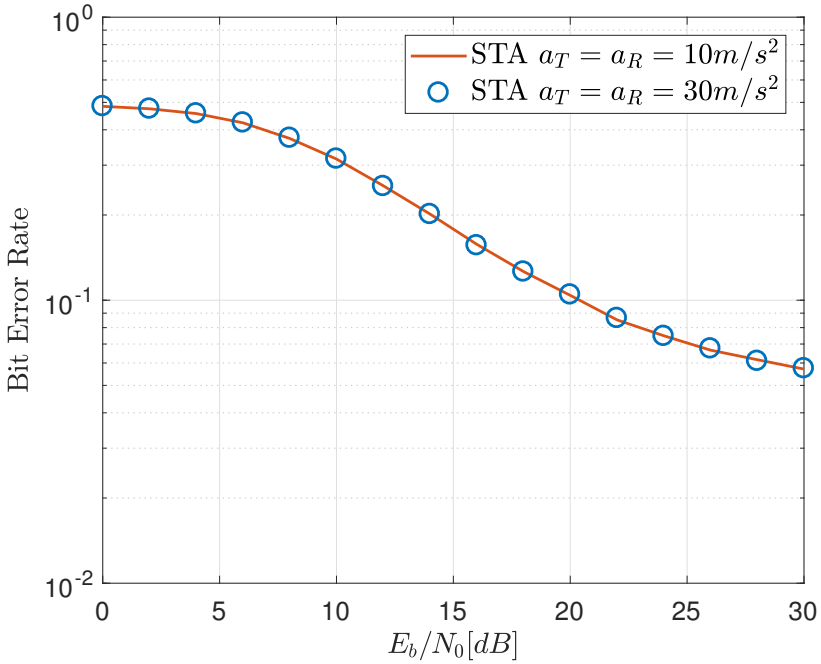

Figure 5.7: BER performance for the STA estimator, for different acceleration values. $D = 300$ m on both curves.

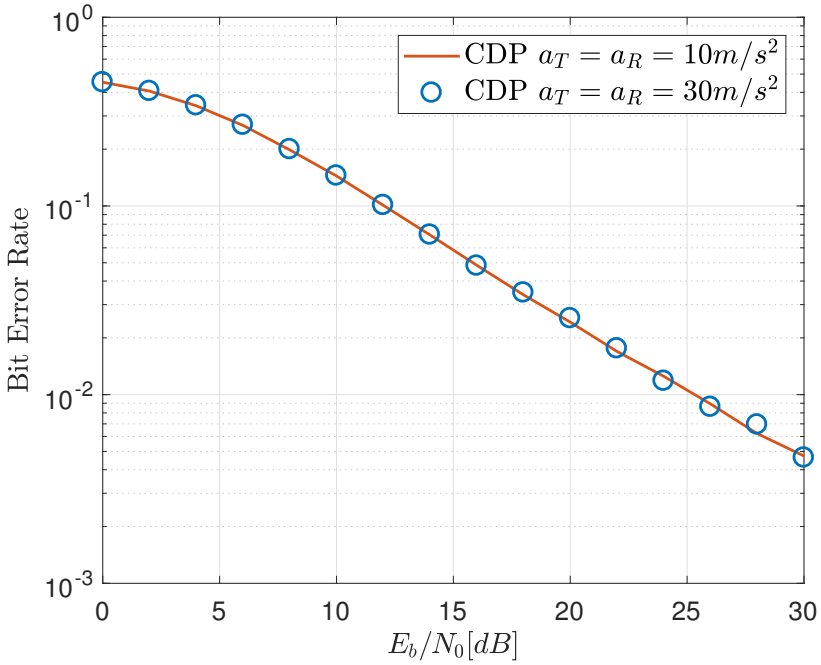

Figure 5.8: BER performance for the CDP estimator, for different acceleration values. $D = 300$ m on both curves.

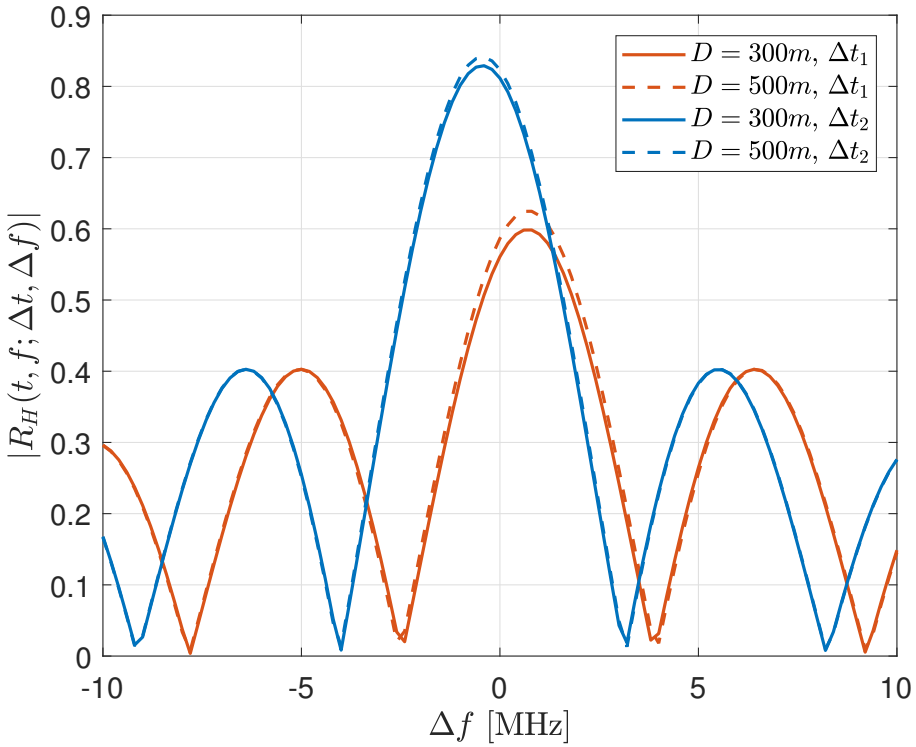

Figure 5.9: 4D TF-CF for observation points ($t = 0{,}5T_0$, $f = 0{,}25B$, $\Delta t_1 = -0{,}92T_0$) and ($t = 0{,}5T_0$, $f = 0{,}25B$, $\Delta t_2 = 0{,}58T_0$). $a_T = a_R = 10$ m/s^2 for both initial distance values.

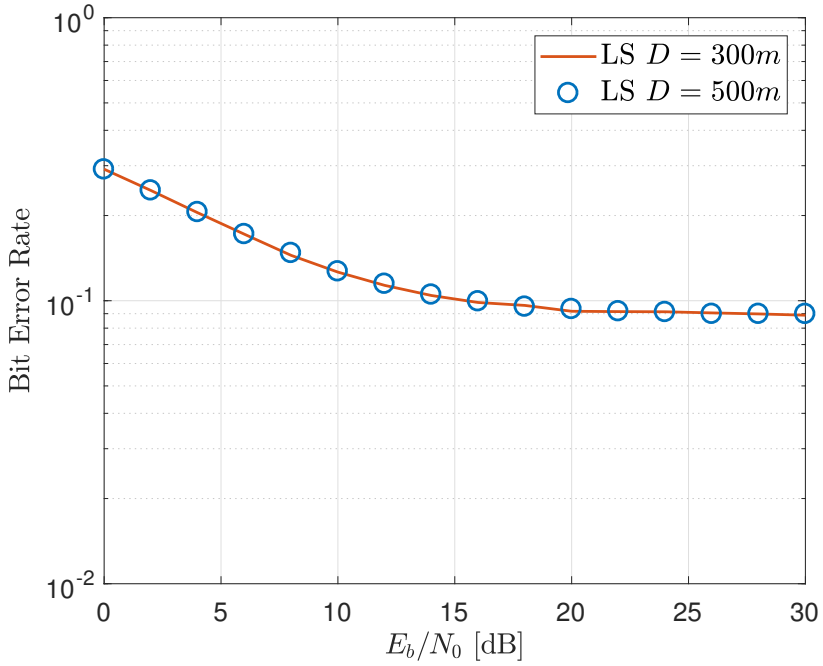

Figure 5.10: BER performance of the LS estimator for different initial distance values. $a_T = a_R = 10$ m/s^2 on both curves.

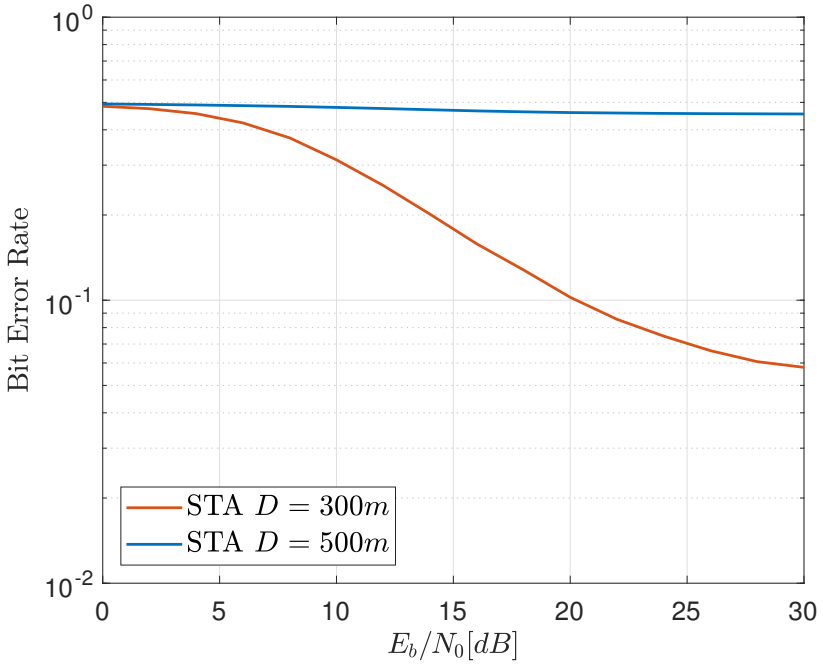

Figure 5.11: BER performance of the STA estimator for different initial distance values. $a_T = a_R = 10$ m/s^2 on both curves.

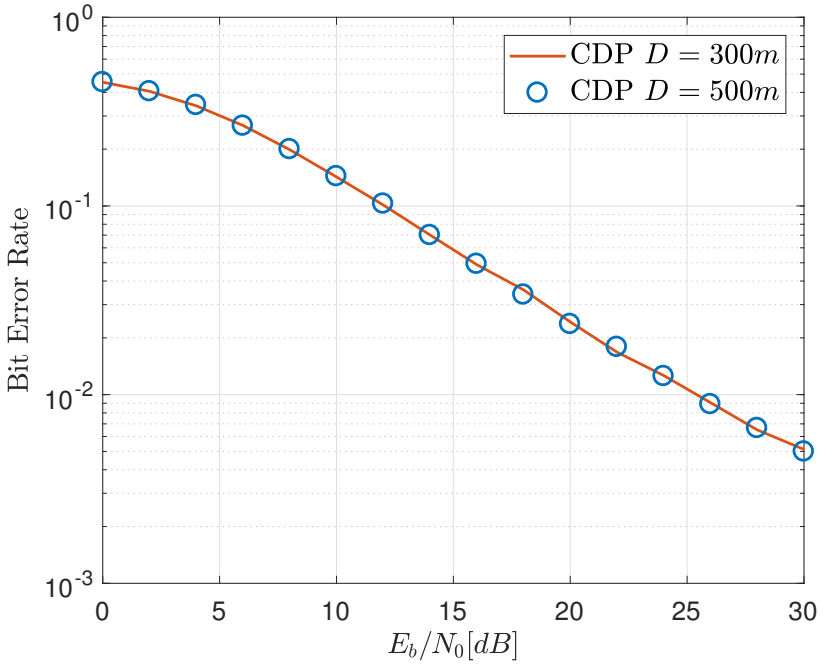

Figure 5.12: BER performance of the CDP estimator for different initial distance values. $a_T = a_R = 10$ m/s^2 on both curves.

Chapter 6

Conclusions and Future Work

Vehicular communications for safety applications are a continuously growing research field. Given these intents for V2V communications, the particular propagation conditions of a vehicular environment should be studied in detail. On this work, we have put our focus on the non-stationary statistics and its impact in the performance of the system. We have detailed study a previously proposed non-WSSUS channel model, which has turn to be very appropriate to simulate vehicular propagation environments. On our statistical characterization of the channel model, we have used a time dependent delay, which is a uncommon practice in the channel modeling literature. The time-domain dependence of the time delays is not an arbitrary decision, in fact, it is turned to be the logical modeling approach to think about it when a vehicular propagation is considered. This latter fact is a natural consequence of the velocities of the mobiles involved in the communication. This time dependence of the time delays has a direct consequence in the modeling of the Doppler Shift, when wideband channels are considered, turning the DS in a time-frequency dependent quantity. In that dependency of the DS, we have found the origins of the non-stationary behaviour of the 4D TF-CF. With all the statistical characterization performed, we focus our efforts on simulations that describe the effect on the BER performance of the system, given the non-stationarities originated from the time-frequency dependence of the DS.

We have shown that the second-order statistics do not vary significantly when the acceleration of the mobiles changes. We also show that an increment on the acceleration of the mobiles has no impact on the BER performance of the system. This lack of variation on the performance is given by the fact that the accelerations are not perceivable on the duration of a single package. Nonetheless, we have shown that the second-order statistics of the channel changes with the initial distance between transmitter and receiver. These variations of the statistics have a strong impact on the performance of the STA estimator. However, the statistics neither impact the performance of the LS, nor the CDP estimator. These latter two estimators are time-domain only techniques, meanwhile, the STA estimator is a time-frequency estimation technique. Given the construction of the channel model, we have also shown that the cause of the non-stationarities is the Doppler effect caused by the accelerated motion of the mobiles. This latter founding is reinforced by the fact that variations on the acceleration of the mobiles do not impact the performance of the STA estimator, but the initial distance between the mobiles do impact the BER performance of this estimation tech-

nique. As it was stated, the channel model used only takes into account small scale fading effects. So, as our geometrical modeling of the time delays involves the distance between the mobiles, and given the relation between the time delays and the DS showed on Chapter 4, we conclude that the non-stationarities caused by the frequency-dependent DS are the main cause of the degradation on the system performance in the case of the STA estimator.

The fact that the Doppler effect degrades the system performance should be taken into account in future work, especially in the design of channel estimation techniques for vehicular environments. As proposed future work, we state that novel techniques designed for vehicular propagation should consider compensation factors that involved knowledge on the DS. We also propose that a detailed mathematical analysis on the relation of BER performance and the second-order statistics should be work of interest. As steps to follow, we propose that a parametrized expression for the BER performance of the LS, CDP and STA estimators should be derived, in order to shed a light on the relationship between the behavior of the second-order statistics, and the BER performance of the system.

Chapter 7

Annexes

Appendix A: Publications and Awards

Journals (ISI/JCR)

- C. A. Gutiérrez, M. Pätzold, **Nicolás M. Ortega**, C. Azurdia-Meza and F. M. Maciel-Barboza, 'Doppler Shift Characterization of Wideband Mobile Radio Channels,' in *IEEE Transactions on Vehicular Technology*, vol. 68, no. 12, pp. 12375 - 12380, Dic. 2019, *doi: 10.1109/TVT.2019.2945936*.

International Conferences

- **Nicolás M. Ortega**, C. A. Azurdia-Meza, C. A. Gutierrez and C. A. Gómez-Vega, 'Second Order Statistics and BER Performance Analysis of a non-WSSUS V2X Channel Model that Considers Velocity Variations,' *in Proc. 2019 IEEE 11th Latin-American Conference on Communications (LATINCOM)*, Salvador, Brazil.
- **Nicolás M. Ortega**, C. A. Azurdia-Meza, C. A. Gutierrez and F. M. Maciel-Barboza, 'On the Influence of the non-WSSUS Condition in the Performance of IEEE 802.11-Based Channel Estimators for Vehicular Communications,' *in Proc. 2018 IEEE 10th Latin-American Conference on Communications (LATINCOM)*, Guadalajara, México.
- P. Palacios, C. A. Azurdia-Meza, **Nicolás M. Ortega**, N. Alonso, 'MIMO Millimeter-Wave Channel Estimation Using Coalitional Games,' in Proc. Spring School on Networks 2018 (SSN), Valdivia, Chile.

Awards

- Best Paper Award given to 'Second Order Statistics and BER Performance Analysis of a non-WSSUS V2X Channel Model that Considers Velocity Variations,' *in Proc. 2019 IEEE 11th Latin-American Conference on Communications (LATINCOM)*, Salvador.

Appendix B: Codes

All the codes used in this work are available in the following link:

`https://github.com/LaboratorioTICs-UChile/`

Chapter 8

Bibliography

[1] F. Qu, F. Y. Wang, and L. Yang, "Intelligent transportation spaces: Vehicles, traffic, communications, and beyond," *IEEE Communications Magazine*, vol. 48, pp. 136–142, Nov. 2010.

[2] L. Li, D. Wen, and D. Yao, "A survey of traffic control with vehicular communications," *IEEE Transactions on Intelligent Transportation Systems*, vol. 15, pp. 425–432, Feb. 2014.

[3] M. Awad, K. Seddik, and A. Elezabi, "Low-Complexity Semi-Blind Channel Estimation Algorithms for Vehicular Communications Using the IEEE 802.11p Standard," *IEEE Transactions on Intelligent Transportation Systems*, vol. PP, pp. 1–10, May 2018.

[4] Z. Zhao, X. Cheng, M. Wen, B. Jiao, and C.-X. Wang, "Channel Estimation Schemes for IEEE 802.11p Standard," *IEEE Inteligent Transportation Systems*, vol. 5, pp. 38–49, Winter 2013.

[5] M. Medard, "The effect upon channel capacity in wireless communications of perfect and imperfect knowledge of the channel," *IEEE Transactions on Information Theory*, vol. 46, pp. 933–946, May 2000.

[6] L. Bernadó, T. Zemen, F. Tufvesson, A. F. Molisch, and C. F. Mecklenbräuker, "The (in-) validity of the WSSUS assumption in vehicular radio channels," in *2012 IEEE 23rd International Symposium on Personal, Indoor and Mobile Radio Communications - (PIMRC)*, pp. 1757–1762, Sept 2012.

[7] A. Roivainen, P. Jayasinghe, J. Meinila, V. Hovinen, and M. Latva-aho, "Vehicle-to-vehicle radio channel characterization in urban environment at 2.3 GHz and 5.25 GHz," in *2014 IEEE 25th Annual International Symposium on Personal, Indoor, and Mobile Radio Communication (PIMRC)*, pp. 63–67, Sept. 2014.

[8] C. A. Gutiérrez, J. T. Gutiérrez-Mena, J. M. Luna-Rivera, D. U. Campos-Delgado, R. Velázquez, and M. Pätzold, "Geometry-Based Statistical Modeling of Non-WSSUS Mobile-to-Mobile Rayleigh Fading Channels," *IEEE Transactions on Vehicular Techno-*

logy, vol. 67, pp. 362–377, Jan. 2018.

[9] C. A. Gutierrez, M. Patzold, W. Dahech, and N. Youssef, "A Non-WSSUS Mobile-to-Mobile Channel Model Assuming Velocity Variations of the Mobile Stations," in *2017 IEEE Wireless Communications and Networking Conference (WCNC)*, pp. 1–6, March 2017.

[10] J. Karedal, F. Tufvesson, N. Czink, A. Paier, C. Dumard, T. Zemen, C. F. Mecklenbräuker, and A. F. Molisch, "A geometry-based stochastic MIMO model for vehicle-to-vehicle communications," *IEEE Transactions on Wireless Communications*, vol. 8, pp. 3646–3657, July 2009.

[11] F. M. Schubert, M. L. Jakobsen, and B. H. Fleury, "Non-stationary propagation model for scattering volumes with an application to the rural LMS channel," *IEEE Transactions on Antennas and Propagation*, vol. 61, pp. 2817–2828, May 2013.

[12] M. Walter, D. Shutin, and U. C. Fiebig, "Delay-dependent doppler probability density functions for vehicle-to-vehicle scatter channels," *IEEE Transactions on Antennas and Propagation*, vol. 62, pp. 2238–2249, Apr. 2014.

[13] J. A. Fernandez, K. Borries, L. Cheng, B. V. K. V. Kumar, D. D. Stancil, and F. Bai, "Performance of the 802.11p physical layer in vehicle-to-vehicle environments," *IEEE Transactions on Vehicular Technology*, vol. 61, pp. 3–14, Jan. 2012.

[14] M. Engels, *Wireless OFDM systems: How to make them work?* Springer Science & Business Media, 2002.

[15] C. A. Gutiérrez, M. Pätzold, N. M. Ortega, C. Azurdia-Meza, and F. M. Maciel-Barboza, "Doppler shift characterization of wideband mobile radio channels," *IEEE Transactions on Vehicular Technology*, pp. 1–1, 2019.

[16] N. M. Ortega, C. A. Azurdia-Meza, C. A. Gutierrez, and F. M. Maciel-Barboza, "On the Influence of the non-WSSUS Condition in the Performance of IEEE 802.11-Based Channel Estimators for Vehicular Communications," in *2018 IEEE 10th Latin-American Conference on Communications (LATINCOM)*, pp. 1–6, Nov 2018.

[17] N. M. Ortega, C. A. Azurdia-Meza, C. A. Gutierrez, and C. Gomez, "Second Order Statistics and BER Performance Analysis of a non-WSSUS V2X Channel Model that Considers Velocity Variations," in *2019 IEEE 11th Latin-American Conference on Communications (LATINCOM)*, pp. 1–6, Nov 2019.

[18] A. Marroquín, M. To De Leon, C. Azurdia-Meza, and S. Bolufe, "A General Overview of Vehicle-to-X (V2X) Beacon-Based Cooperative Vehicular Networks," in *2019 IEEE 39th Central America and Panama Convention (CONCAPAN XXXIX)*, pp. 1–6, Nov 2019.

[19] Y. Toor, P. Muhlethaler, A. Laouiti, and A. D. La Fortelle, "Vehicle ad hoc networks: applications and related technical issues," *IEEE Communications Surveys Tutorials*, vol. 10, pp. 74–88, Third 2008.

[20] "IEEE standard for information technology–telecommunications and information exchange between systems local and metropolitan area networks–specific requirements part 11: Wireless LAN medium access control (MAC) and physical layer (PHY) specifications," *IEEE Std 802.11-2012 (Revision of IEEE Std 802.11-2007)*, pp. 1–2793, March 2012.

[21] A. Abdelgader and L. Wu, "The Physical Layer of the IEEE 802.11p WAVE Communication Standard: The Specifications and Challenges," vol. 2, 10 2014.

[22] V. Savaux and Y. Louët, "LMMSE channel estimation in OFDM context: a review," *IET Signal Processing*, vol. 11, pp. 123–134, Apr. 2017.

[23] Y. Ren, D. C. Park, and S. C. Kim, "A novel channel estimation scheme for IEEE 802.11p in VANET," in *2015 Seventh International Conference on Ubiquitous and Future Networks*, pp. 435–437, July 2015.

[24] M. M. Awad, K. G. Seddik, and A. Elezabi, "Channel estimation and tracking algorithms for harsh vehicle to vehicle environments," in *2015 IEEE 82nd Vehicular Technology Conference (VTC2015-Fall)*, pp. 1–5, Sept. 2015.

[25] J. A. Fernandez, D. D. Stancil, and F. Bai, "Dynamic channel equalization for IEEE 802.11p waveforms in the vehicle-to-vehicle channel," in *2010 48th Annual Allerton Conference on Communication, Control, and Computing (Allerton)*, pp. 542–551, Sept. 2010.

[26] T. Rappaport, *Wireless Communications: Principles and Practice*. Upper Saddle River, NJ, USA: Prentice Hall PTR, 2nd ed., 2001.

[27] W. C. Jakes and D. C. Cox, eds., *Microwave Mobile Communications*. Wiley-IEEE Press, 1994.

[28] M. Patzold, *Mobile Fading Channels*. New York, NY, USA: John Wiley & Sons, Inc., 2003.

[29] W. L. Stutzman and G. A. Thiele, *Antenna Theory and Design*. John Wiley Sons, 1998.

[30] G. Matz, "On non-WSSUS wireless fading channels," *IEEE Transactions on Wireless Communications*, vol. 4, pp. 2465–2478, Sep. 2005.

[31] R. Yates, *Probability and Stochastic Processes: A Friendly Introduction for Electrical and Computer Engineers, 3rd Edition: Third Edition*. Probability and Stochastic Processes: A Friendly Introduction for Electrical and Computer Engineers, John Wiley & Sons, 2014.

[32] A. Abdi, J. A. Barger, and M. Kaveh, "A parametric model for the distribution of the angle of arrival and the associated correlation function and power spectrum at the mobile station," *IEEE Transactions on Vehicular Technology*, vol. 51, pp. 425–434, May 2002.

[33] I. S. Gradshteyn and I. M. Ryzhik, *Table of integrals, series, and products*. Elsevier/Academic Press, Amsterdam, seventh ed., 2007. Translated from the Russian, Translation

edited and with a preface by Alan Jeffrey and Daniel Zwillinger, With one CD-ROM (Windows, Macintosh and UNIX).

[34] B. Boashash, "Estimating and interpreting the instantaneous frequency of a signal. I. fundamentals," *Proceedings of the IEEE*, vol. 80, pp. 520–538, April 1992.

[35] W. Dahech, M. Pätzold, C. A. Gutiérrez, and N. Youssef, "A non-stationary mobile-to-mobile channel model allowing for velocity and trajectory variations of the mobile stations," *IEEE Transactions on Wireless Communications*, vol. 16, pp. 1987–2000, March 2017.

[36] M. Walter, D. Shutin, and A. Dammann, "Time-variant Doppler PDFs and Characteristic Functions for the Vehicle-to-Vehicle Channel," *IEEE Transactions on Vehicular Technology*, vol. 66, pp. 10748–10763, Dec 2017.

[37] Y. Shmaliy, *Continuous-Time Systems*. Signals and Communication Technology, Springer Netherlands, 2007.

[38] B. Li, S. Zhou, M. Stojanovic, L. Freitag, and P. Willett, "Multicarrier Communication over Underwater Acoustic Channels with Nonuniform Doppler Shifts," *IEEE Journal of Oceanic Engineering*, vol. 33, pp. 198–209, April 2008.

[39] J. J. J. Rodriguez, *Modeling , Analysis , and Simulation of non-WSSUS Vehicle-to-Vehicle Channels*. PhD thesis, Universidad Autónoma de San Luis de Potosí, San Luis de Potosí, 2018.

[40] Y. Yang, D. Fei, and S. Dang, "Inter-vehicle cooperation channel estimation for IEEE 802.11p V2I communications," *Journal of Communications and Networks*, vol. 19, pp. 227–238, July 2017.

[41] Y. Liu, Z. Tan, H. Hu, L. J. Cimini, and G. Y. Li, "Channel Estimation for OFDM," *IEEE Communications Surveys & Tutorials*, vol. 16, pp. 1891–1908, May 2014.

[42] Y.-K. Kim, J.-M. Oh, Y.-H. Shin, and C. Mun, "Time and frequency domain channel estimation scheme for IEEE 802.11p," in *17th International IEEE Conference on Intelligent Transportation Systems (ITSC)*, pp. 1085–1090, Oct. 2014.

[43] J. Chen and T. G. Pratt, "Three-dimensional geometry-based stochastic modeling and performance of 44 space-polarization mobile-to-mobile wideband MIMO channels," *GLOBECOM - IEEE Global Telecommunications Conference*, pp. 3936–3941, 2013.

[44] A. Zajic, G. Stuber, T. Pratt, and S. Nguyen, "Wideband MIMO mobile-to-mobile channels: geometry based statistical modeling with experimental verification," *IEEE Vehicular Technology Magazine*, vol. 58, no. 2, pp. 517–534, 2009.

[45] Taewon Hwang, Chenyang Yang, Gang Wu, Shaoqian Li, and G. Ye Li, "OFDM and Its Wireless Applications: A Survey," *IEEE Transactions on Vehicular Technology*, vol. 58, no. 4, pp. 1673–1694, 2009.

[46] M. K. Ozdemir and H. Arslan, "Channel Estimation for Wireless OFDM Systems," *IEEE Communications Surveys*, vol. 9, pp. 18–48, July 2007.

[47] J. Shapiro, "Smart cities: quality of life, productivity, and the growth effects of human capital," *The review of economics and statistics*, vol. 88, pp. 324–335, May 2006.

[48] X. Ge, H. Cheng, G. Mao, Y. Yang, and S. Tu, "Vehicular Communications for 5G Cooperative Small-Cell Networks," *IEEE Transactions on Vehicular Technology*, vol. 65, pp. 7882–7894, Oct. 2016.

[49] J. J. Rodríguez *et al.*, "A Monte Carlo simulator of non-WSSUS Rayleigh fading channels for vehicular communications," in *Proc. of the 38th IEEE Convention of Central America and Panama (CONCAPAN XXXVIII)*, (San Salvador, El Salvador), pp. 1–6, 2018.

[50] C. A. Gómez-Vega, J. J. Jaime-Rodríguez, C. A. Gutiérrez, and R. Velázquez, "Bit error rate performance analysis of vehicular communication systems considering velocity variations of the mobile stations," in *2017 IEEE 37th Central America and Panama Convention (CONCAPAN XXXVII)*, pp. 1–6, Nov 2017.